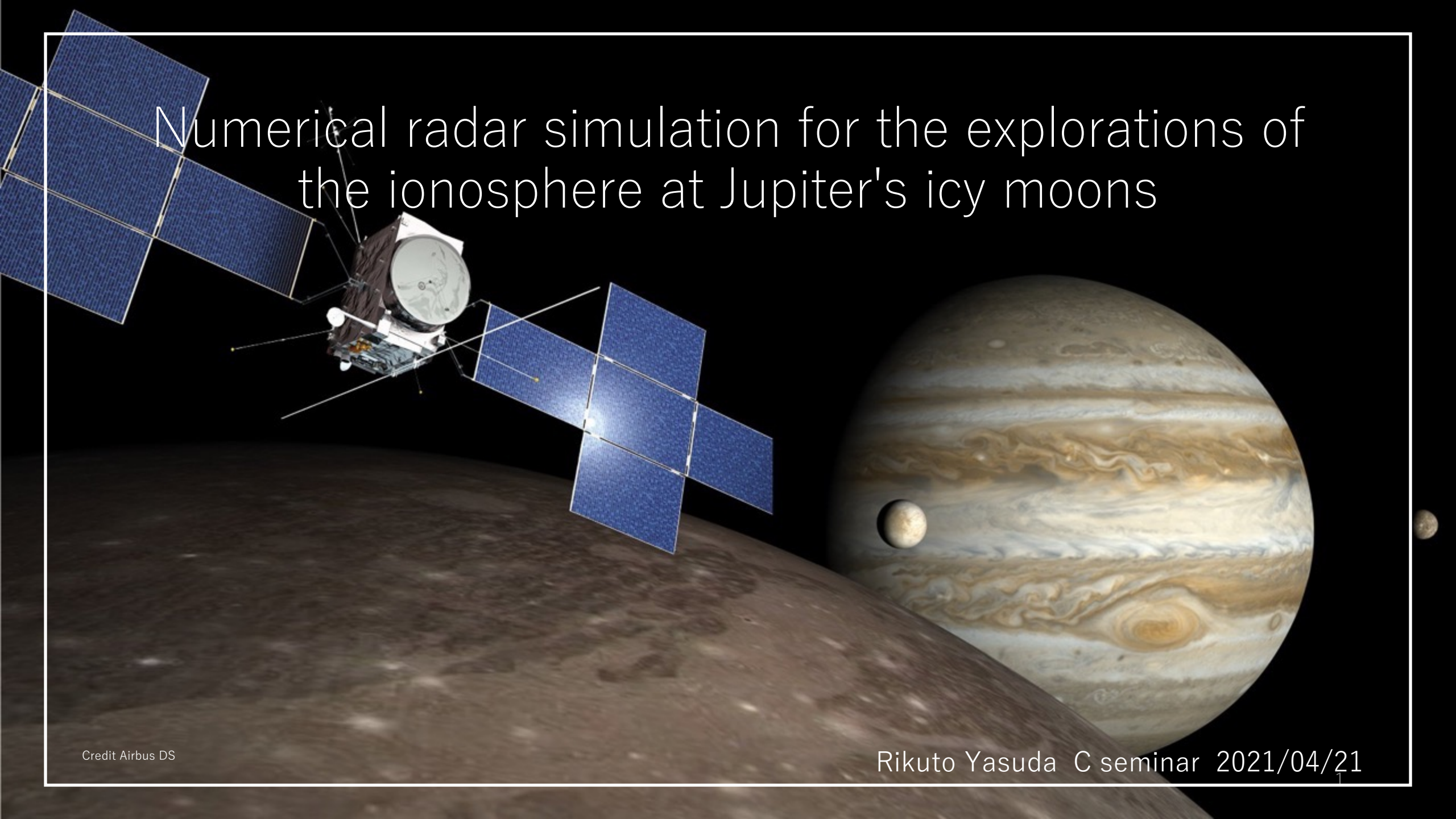


Numerical radar simulation for the explorations of the ionosphere at Jupiter's icy moons



1. Introduction

1-1 [Jupiter's icy moon](#)

1-2 [Ionosphere of Jupiter's icy moon](#)

1-3 Previous observation of moon's ionosphere electron density

[1-3-1 Ganymede ionosphere](#)

[1-3-2 Europa ionosphere](#)

[1-3-3 Calisto ionosphere](#)

[1-3-4 Problems with the previous observation methods](#)

1-4 [Preceding studies of Jovian radio emission occultations](#)

1-5 [Purpose of this study](#)

2. Method

2-1. How to combine Raytracing method with Radio Emission
Simulations

2-2 Raytracing

2-3 Verify time-step validity of raytracing code

2-4 Ionosphere model and evaluation method

3. Radio occultation observation

3-1 Ganymede ionosphere result

3-2 Discussion of Ganymede ionosphere results

3-3 Europa ionosphere result

3-4 Discussion of Europa ionosphere results

4. Conclusion

5. Future works

1-1. Jupiter's icy moon

~ Jupiter's icy moon ~

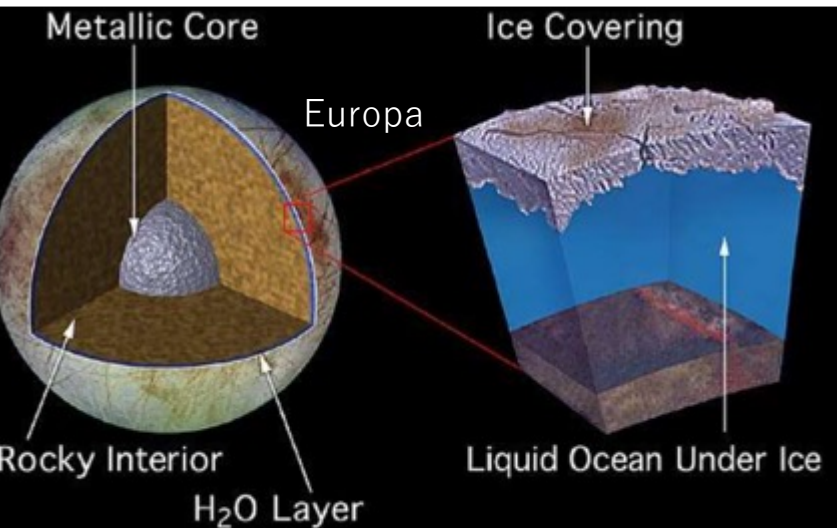
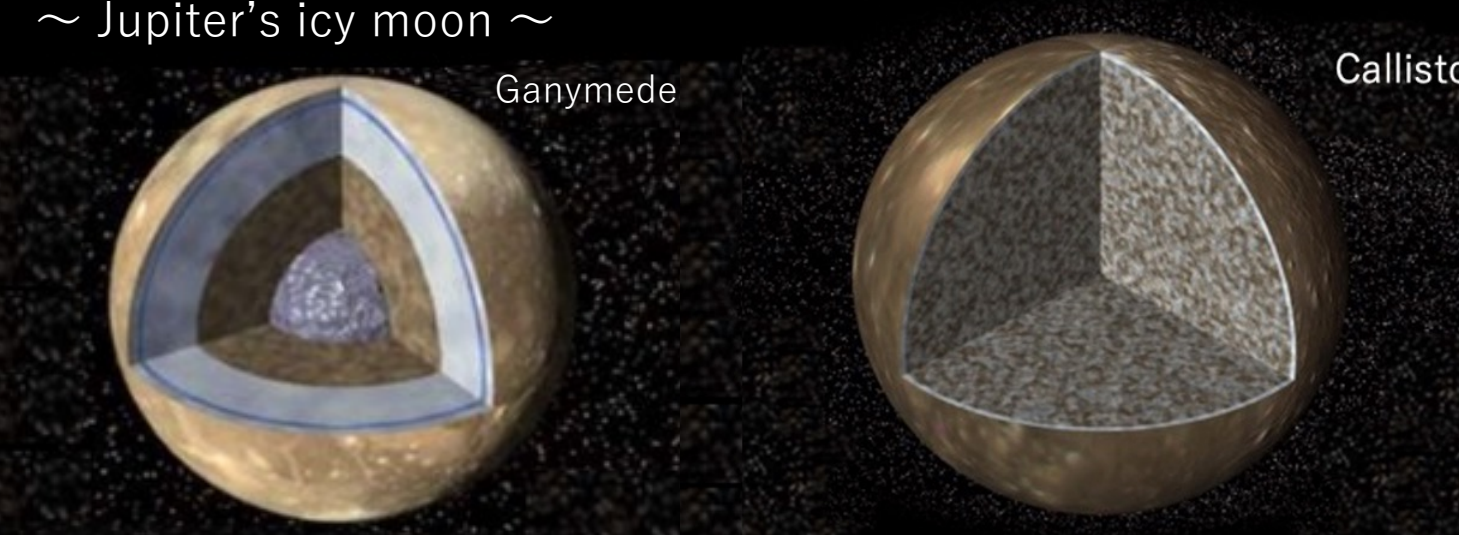


Fig.4 Model interiors of Ganymede Callisto and Europa [Schubert et al, 2004]

Jupiter's icy moon (ex. Europa, Ganymede, Callisto)

- possess internal liquid-water oceans [[Khurana et al., 1998](#); [Kivelson et al., 2002](#) etc..]
- Multiple icy bodies have subsurface ocean while only Earth has surface ocean.

Structures of the interior, ionosphere and plume of the icy moons are essential information for understanding universality of habitable environment.

It is impossible to observe directly ionosphere and plumes at low altitude as well as interiors.

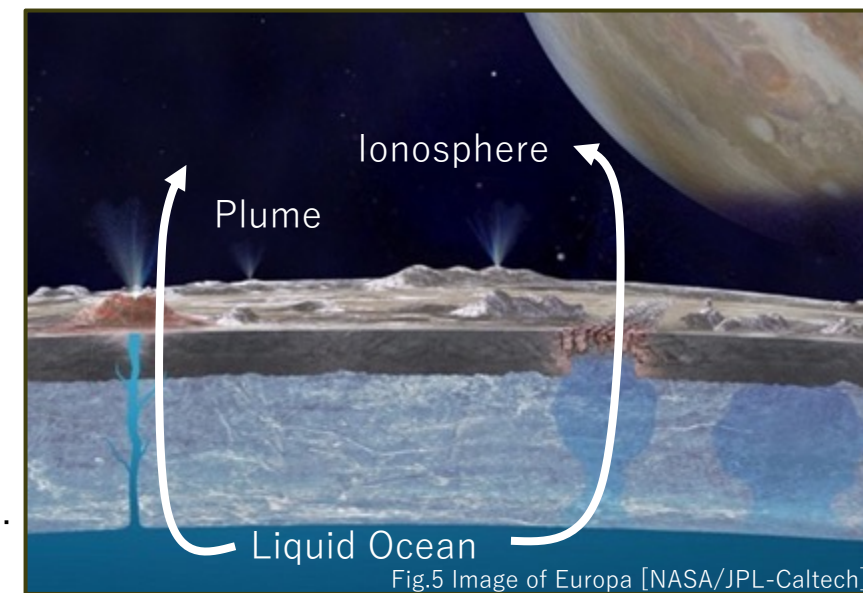


Fig.5 Image of Europa [NASA/JPL-Caltech]

JUICE (JUpiter ICy moons Explorer)

Radio and Plasma Wave Investigation (RPWI) [Frequency: 80kHz~45MHz]

- ... A radio plasma wave instrument to characterize radio emission and plasma environment
- Apply to radio occultation observation or passive radar. (Fig.4, 5)

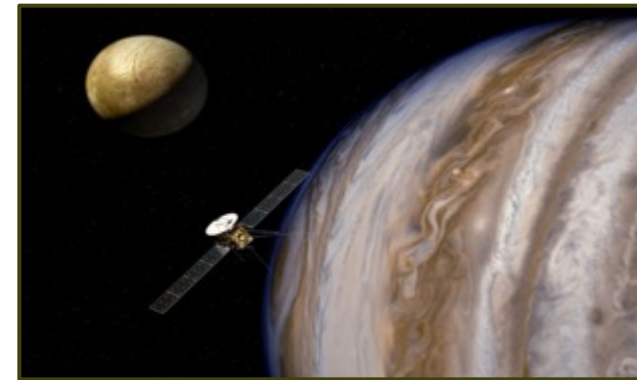


Fig.6 JUICE [Airbus DS]

① Radio occultation observation of the ionosphere

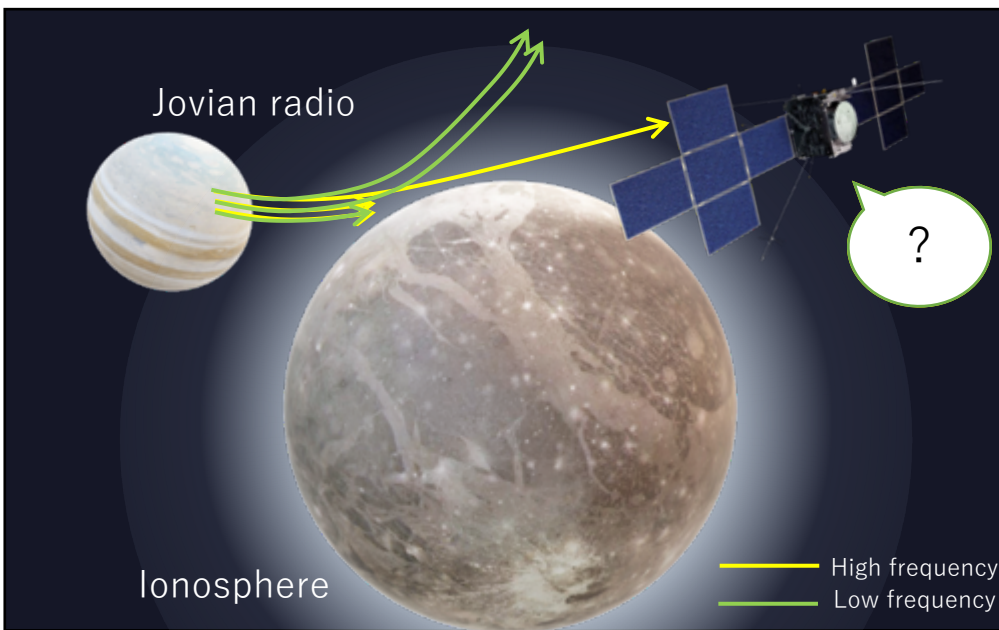


Fig.7 Radio observation using Jovian radio refraction
(adapted from Airbus DS and NASA/JPL)

② Passive radar

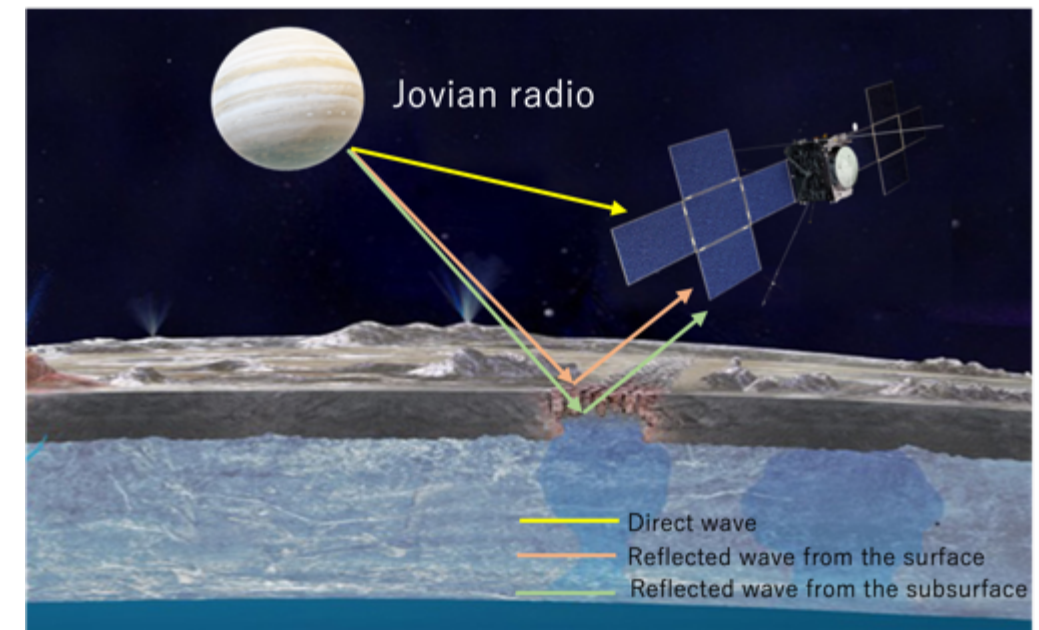
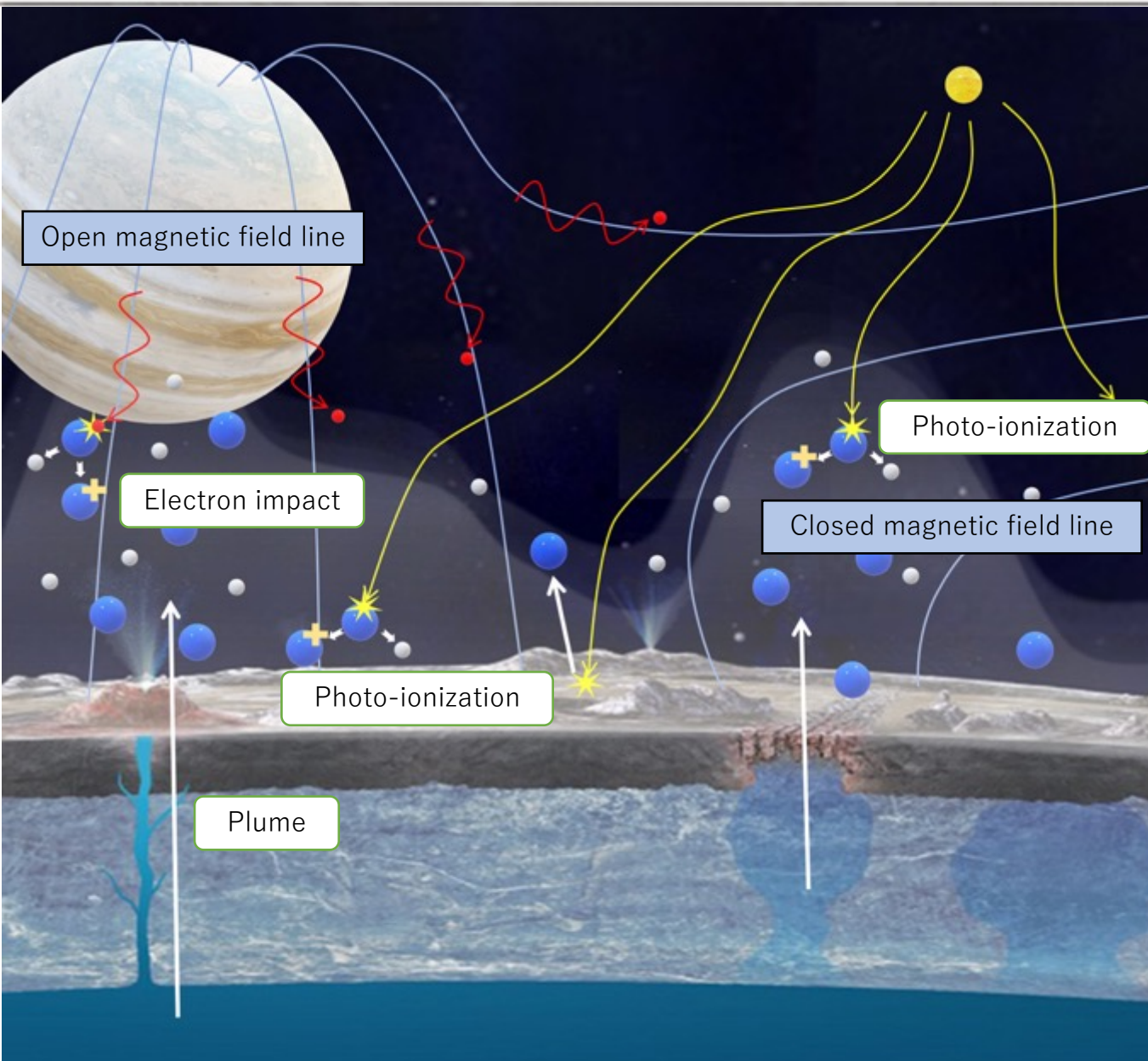


Fig.8 Radio observation using Jovian radio reflection
(adapted from NASA/JPL, Airbus DS and gcoe-earths.org)

1-2. Ionosphere of Jupiter's icy moon



Ionization source ([Carnielli et al. \(2019\)](#))

① Photo-ionization

exosphere is constantly photo-ionized by solar EUV radiation

② Electron impact

the energetic electrons (> tens of eV) are able to ionize the neutral exosphere.

Ionosphere structure of icy moons



- Distribution of neutral atmosphere (and plume) created from oceanic water materials
- Solar photo-ionization rate and electron impact ionization rate (Energy sources into icy moon)
- Open or closed magnetic field line (Ganymede)

- ionization
- atmosphere supply
- energetic electron supply
- solar EUV
- magnetic field line

- electron of icy moon's ionosphere
- energetic electron
- atmosphere of icy moon
- ionized atmosphere

Fig.9 Ionization process of icy moon
(adapted from NASA/JPL, Airbus DS and gcoe-earths.org)

1-3-1. Ganymede ionosphere

In-situ observation of Galileo flyby [Galileo plasma-wave instrument] (Fig.7 & 8)

	Maximum densities	Scale height	
Gurnett et al. 1996	~ 100 (/cc)	~1000 km	G1
Eviatar et al. 2001a	~ 400 (/cc)	~600 km	G1&G2
Eviatar et al. 2001b	~ 2500 (/cc)	~125km (near Ganymede) ~600 km (farther out)	G2

Fig.12 Proposed maximum electron densities and scale height of Ganymede ionosphere

Radio occultation [Galileo]

Maximum electron densities ... **~4000/cc** ([Kliore 1998](#))

Observation	Lat (deg)	W. Long (deg)	SZA (deg)	Ram Angle (deg)
Ganymede 8 entry	41	201	82	69
Ganymede 8 exit	47	22	98	112

Cf. Fig.13 Geometry of Galileo occupations by Ganymede.

~ in **the region of closed magnetic field lines** we would expect mainly **low energy electrons** to be present from **photo-ionization** of the neutral atmosphere, and not energetic electrons from the Jovian plasma sheet which are not able to penetrate ~



Electron density distribution of ionosphere → What is the origin of Ganymede ionosphere?

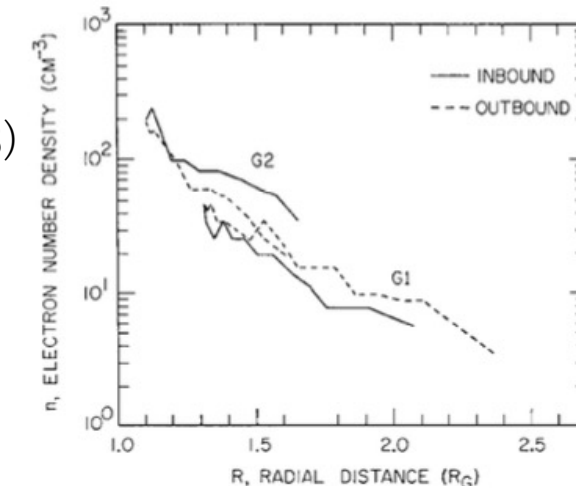


Fig.10 Electron density profiles on Ganymede 2 obtained by means of the PWS instrument on Galileo (Eviatar et al. 2001a)

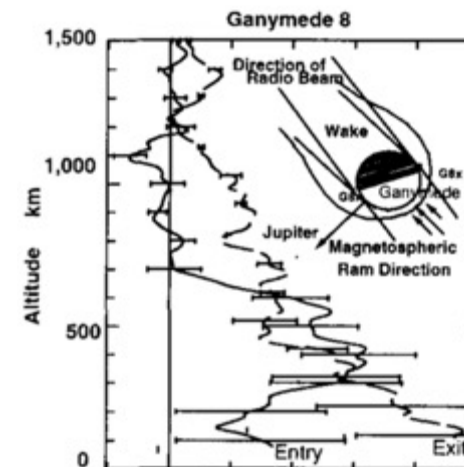


Fig.14 Electron density profiles for Ganymede (Kliore 1998)

1-3-3. Europa ionosphere

Radio occultation [Galileo] ([Kliore et al. \(1997\)](#))

Maximum electron densities ... $9000 \pm 4000/\text{cc}$

Scale height ... $240 \pm 40 \text{ km} (\sim 300 \text{ km})$
 $440 \pm 60 \text{ km} (300 \text{ km} \sim)$

Strong detection ... 5 times

Weak detection ... 1 times

Nondeletion ... 2 times



[Kliore et al. \(2001\)](#)

- in order for an ionosphere to be observed, the trailing hemisphere of the satellite **must be in sunlight**
- the atmosphere created by sputtering effects of the Jovian magnetosphere can be **ionized by solar EUV to produce an observable ionosphere.**



- the electron impact ionization rate is $1.9 \times 10^{-6} \text{ s}^{-1}$ & a solar maximum photoionization rate is $3 \times 10^{-8} \text{ s}^{-1}$ ([Saur et al. \(1998\)](#))
- It is therefore very difficult to understand why the existence of an ionosphere should depend on solar illumination. ([McGrath et al. \(2009\)](#))

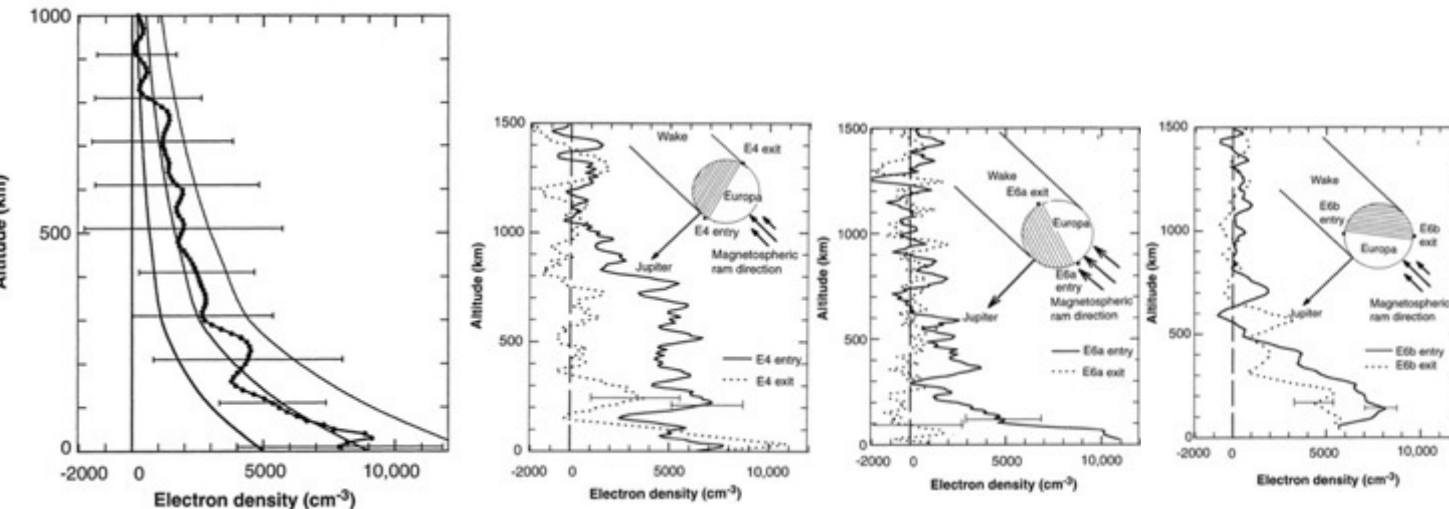


Fig.16 Average Europa electron density profile computed from the five observations in which an ionosphere was detected.(Kliore et al. 1997)

Fig.17 Electron density profiles for Europa. (E4, E6a and E6b) (Kliore et al. 1997)

Occultation modeling using ExPRES Jovian Radio Emission Simulations [Cecconi et al, 2021]

※ Assuming a straight-line propagation (no refraction)

- At lower frequencies, the occultation spectral egress occurs later than predicted. (Fig. 10)
- This prediction mismatch indicates that propagation effects play an important role in the fine understanding of the radio occultation near Galilean moons.

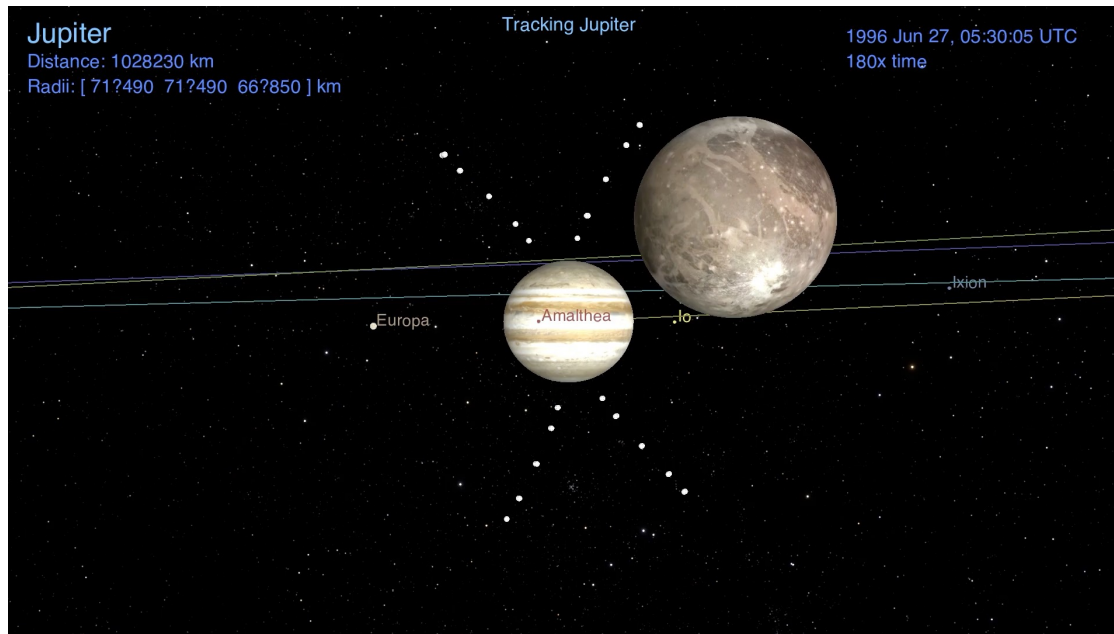


Fig.21 Flyby visualized in the Cosmographia tool. The scene is set with an observer on the Galileo spacecraft, pointing to Jupiter. Ganymede is in the field of view. The ExPRES-modelled visible radio sources are also shown, at 700 kHz, 1 MHz, 2 MHz, 5 MHz and 10 MHz as white dots. The radio sources are conventionally grouped in four sets (named A, B, C and D). [Cecconi et al, 2021]

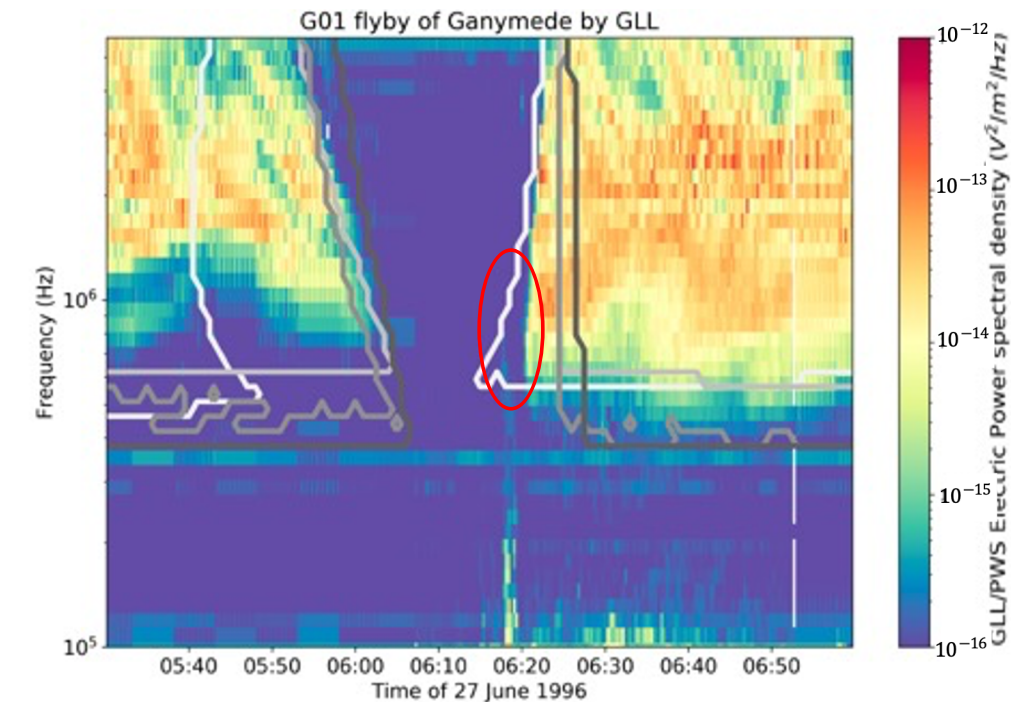


Fig.22 Superimposed Galileo PWS data and ExPRES simulations during Jovian radio emission occultations by Ganymede . The four types of emission (A, B, C, D) are separated (from white to darkgrey, resp.) [Cecconi et al, 2021]

- To investigate spatial structures of ionosphere and plumes created from the water oceanic materials, developing the numerical simulation code for the radar explorations using natural radio waves. [Fig. 4]
(Collaborative research with institutions in France and Sweden)
- Finally, we will also investigate spatial structures of the interior. [Fig. 5]

① Radio occultation observation of the ionosphere

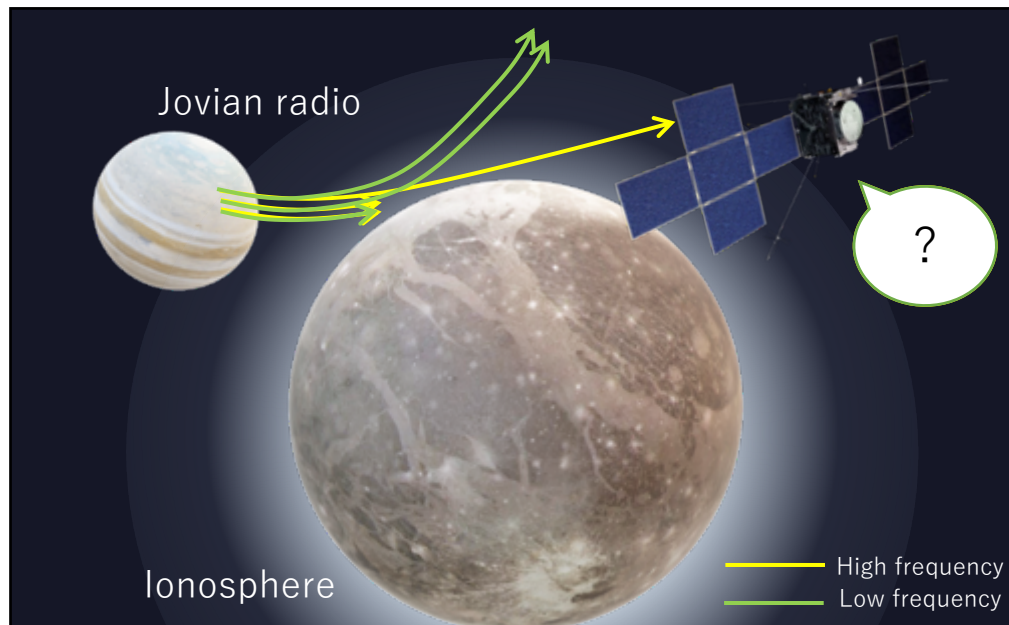


Fig.7 Radio observation using Jovian radio refraction (adapted from Airbus DS and NASA/JPL)

② Passive radar

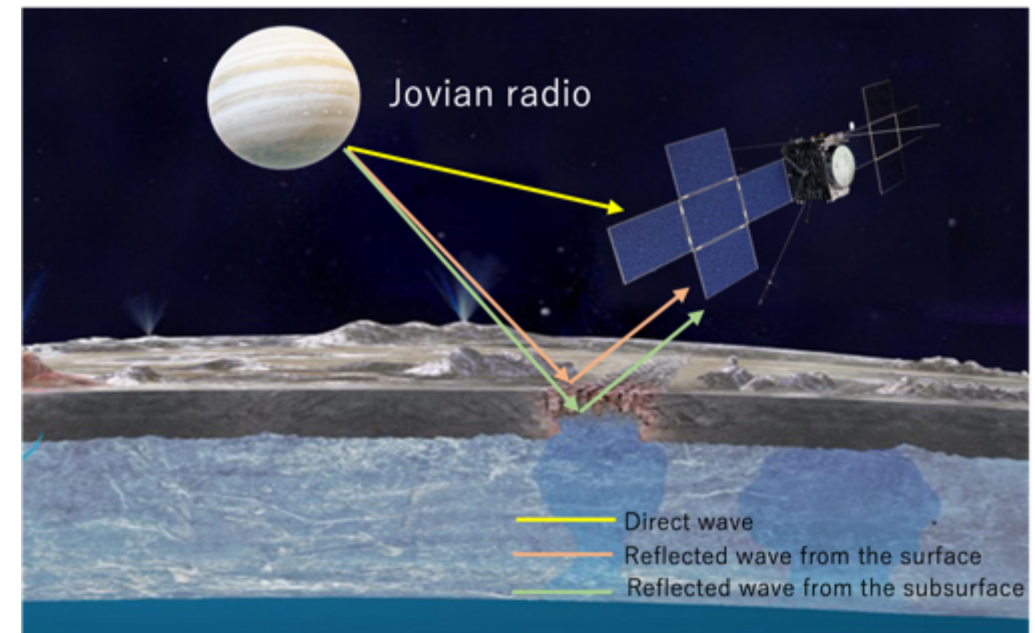


Fig.8 Radio observation using Jovian radio reflection (adapted from NASA/JPL, Airbus DS and gcoe-earths.org)

Today's topic..

- Emulate occultation of the Jovian radio waves during the flybys of the Galileo spacecraft to Ganymede including the ionospheric refraction effect**
- Propose the vertical ionospheric profiles at the altitude below the orbiter**

ExPRES Jovian Radio Emission Simulations

Ephemeris of the observer

↓

The position of the radio sources (➡ in Fig.8)
(The radio is emitted in the direction of the observer)

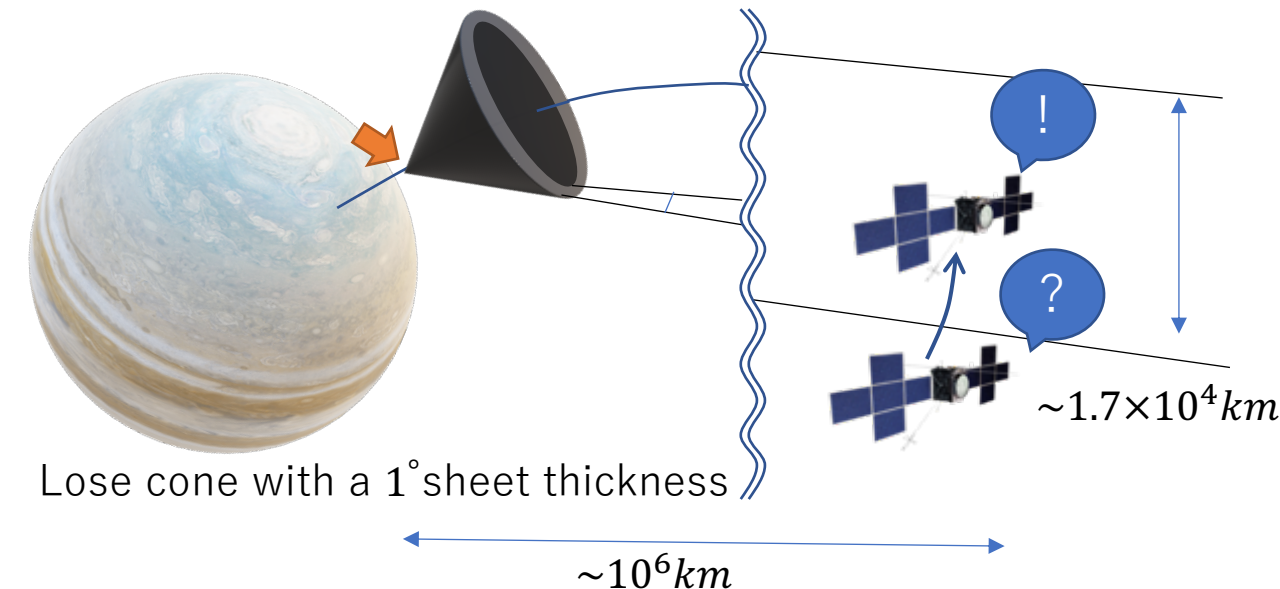


Fig.23 The position of the radio source and the direction of the radio emission
(adapted from Airbus DS and NASA/JPL)

To simulate refraction of Jovian radio waves

Assuming the radio waves are ..

- plane waves
- refracting only in the ionosphere of Ganymede



Fig.24 Initial positions (\vec{r}_0) and Initial wave vectors (\vec{k}_0) of the radio waves in our raytracing code

- In numerical radar simulation, full wave simulation is general method.

ex) FDTD (Finite-difference time-domain method) method (Fig.13)
 ... Solving Maxwell's equations on a mesh and computing E and H at grid points spaced Δx , Δy , and Δz apart.

- However, this method needs high calculation cost when we execute the program in a wide calculation space such as ionosphere, plumes and interiors of icy moons.

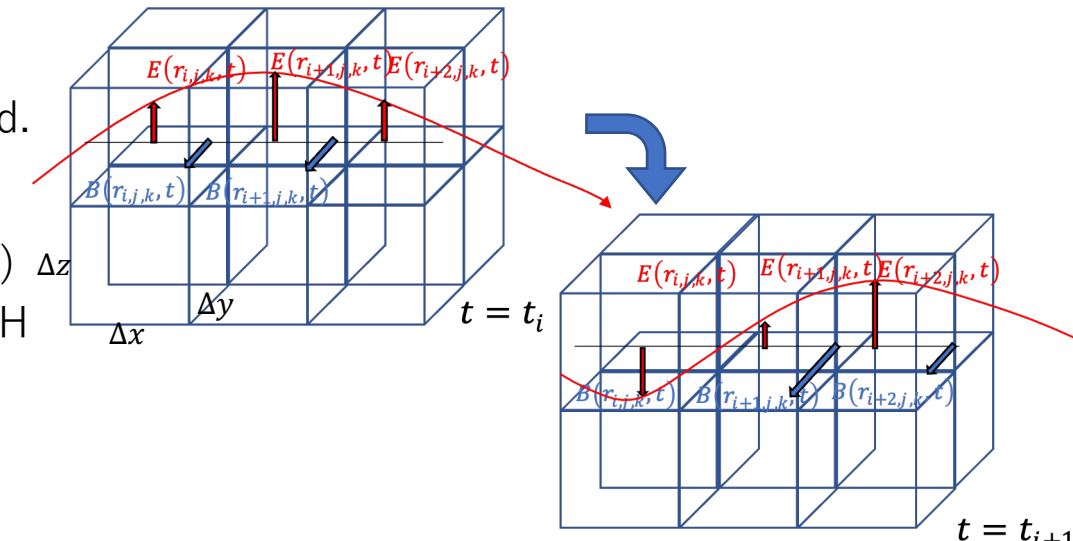


Fig.25 FTDT image

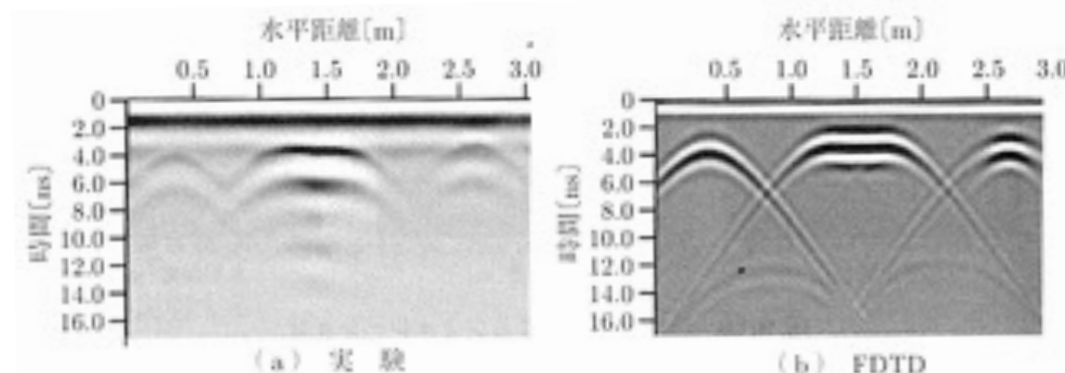


Fig.26 FTDT result [Principles of radar (Kazuo Ouchi)]

Ray tracing ..

more computationally efficient to trace propagation paths of electromagnetic waves in the magnetized plasma, sequentially solving the dispersion relation for plasma waves.

~ input parameter ~

- Magnetic field model $\omega_c(\vec{r}, t)$
- Plasma density model $\omega_p(\vec{r}, t)$
- Frequency of wave (ω)
- Initial position (\vec{r}_0)
- Initial wave vector (\vec{k}_0)



$d\vec{r}_{j+1}$ and $d\vec{k}_{j+1}$ in dt_j

$$(1) \rightarrow d\vec{r}_{j+1} = -\frac{\partial D_j / \partial \vec{k}_j}{\partial D_j / \partial \omega} \cdot dt_j, \quad d\vec{k}_{j+1} = +\frac{\partial D_j / \partial \vec{r}_j}{\partial D_j / \partial \omega} \cdot dt_j$$



the time (t_{j+1}), position (\vec{r}_{j+1}) and wave vector (\vec{k}_{j+1}) after dt_j

- $t_{j+1} = t_j + dt_j$
- $\vec{r}_{j+1} = \vec{r}_j + d\vec{r}_{j+1}$
- $\vec{k}_{j+1} = \vec{k}_j + d\vec{k}_{j+1}$



~ output ~

a full ray path and time ($\vec{r}(t)$)

- Equation of motion of plasma

$$\frac{d\vec{v}}{dx} = \frac{q}{m} (\vec{E} + \vec{v} \times \vec{B})$$

- Maxwell's equations

$$\nabla \times \vec{H} = \vec{j} + \frac{\partial \vec{D}}{\partial t} \quad \nabla \times \vec{E} = -\frac{\partial \vec{B}}{\partial t}$$



(Cold plasma · Discarding plasma collision)

Appleton-Hartree equation (Cf. Appendix A)

~The dispersion relation of waves in magnetized cold plasma~

$$D(t, \vec{r}, \omega, \vec{k}) = \left(\frac{c|\vec{k}|}{\omega} \right)^2 + \frac{2X}{2 - \frac{Y^2 \sin^2 \theta}{1-X} + \rho \sqrt{\frac{Y^2 \sin^4 \theta}{(1-X)^2} + 4Y^2 \cos^2 \theta}} - 1 = 0 \quad \dots (1)$$

$$X = \left(\frac{\omega_p}{\omega} \right)^2 \quad Y = \frac{\omega_c}{\omega} \quad \rho = \text{LO mode : 1, RX mode : -1}$$

\vec{r}, t : position of a ray path and time

θ : an angle between wave normal vector and the local magnetic field vector

ω_p : plasma frequency (depending on plasma density)

ω_c : cyclotron frequency (depending on magnetic field)

Evaluation method

- ① Emulate the Jovian radio waves using ExPRES results and Raytracing with the hydrostatic equilibrium plasma model (Fig.27)
- ② Judge whether the radio sources are visible or not (Make f-t diagrams)
- ③ Check the time to finish receiving radio waves (occultation start) and the time to start receiving radio waves (occultation end) for each frequency
- ④ Examine the time lag between the occultation start/end time and our expected time for each frequency
- ⑤ Calculate the average time lag for each frequency
- ⑥ Repeat ①~⑤ with changing the maximum density and scale height of the hydrostatic equilibrium plasma model
- ⑦ Examine parameter sets when the average time lag is less than 30 sec

~Ganymede ionosphere model~

Plasma density model (Fig.10)

... Hydrostatic equilibrium plasma

Magnetic field model

... Almost zero magnetic field

$(1.0 \times 10^{-11} \text{ (T)} \cdot \text{x-axis direction} \cdot \text{uniformly})$

※ $f_c < f$ at Ganymede surface

(f_c ... Cyclotron frequency, f ... Frequency of waves)

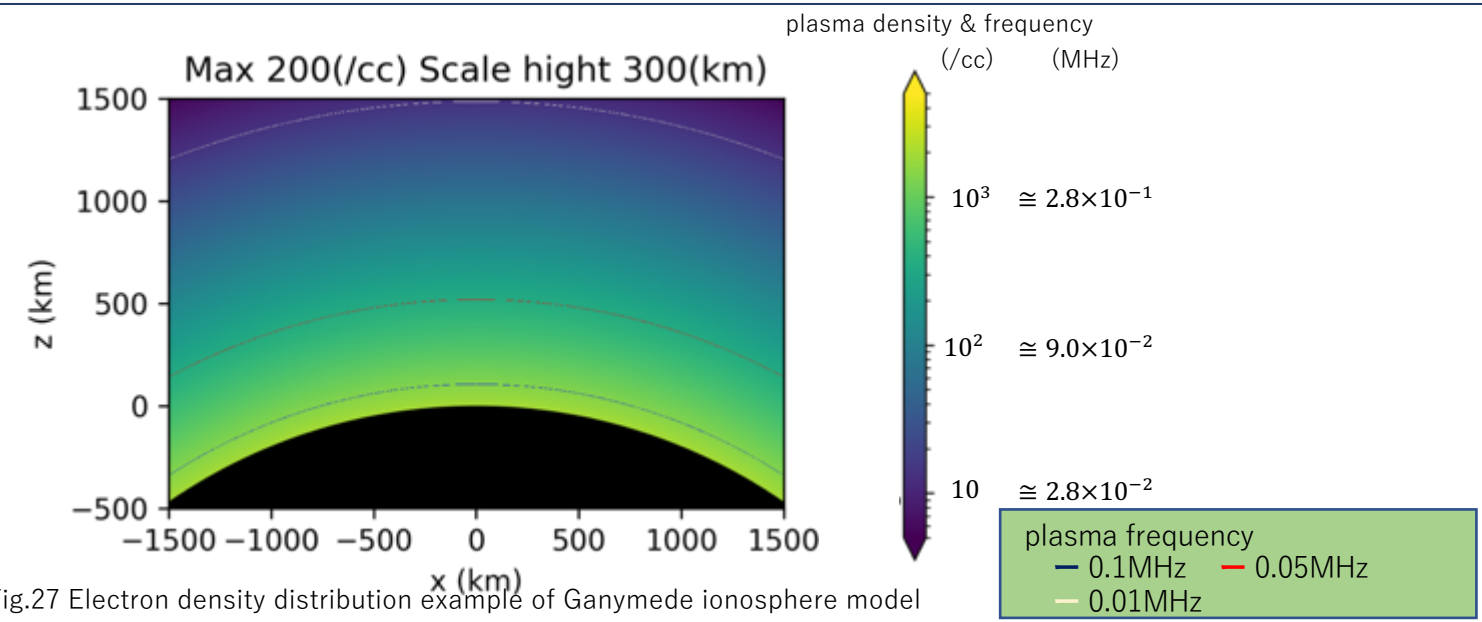
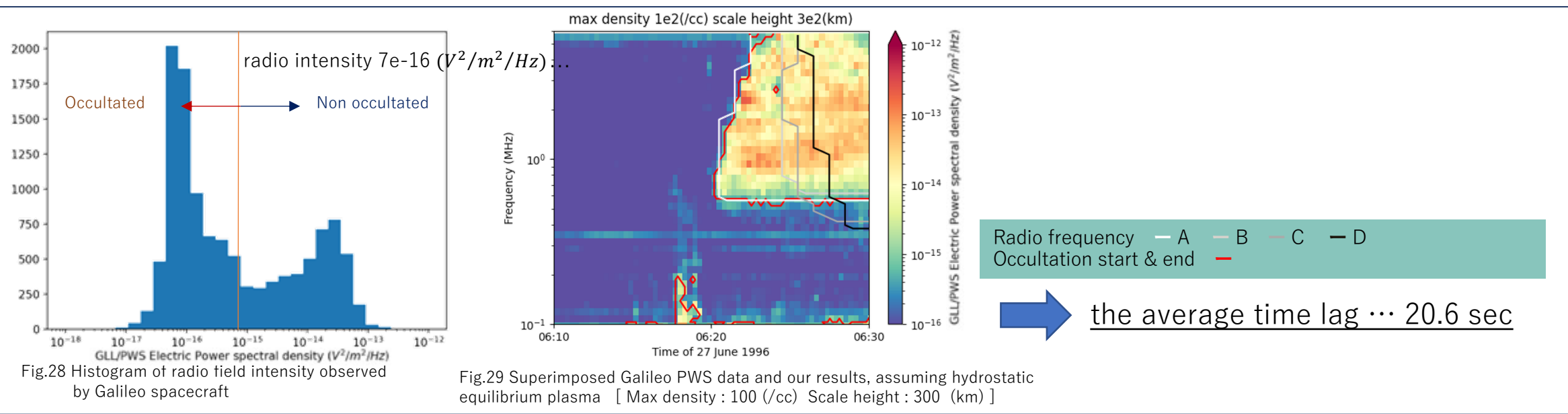


Fig.27 Electron density distribution example of Ganymede ionosphere model

Evaluation method

- ① Emulate the Jovian radio waves using ExPRES results and Raytracing with the hydrostatic equilibrium plasma model (Fig.)
- ② Judge whether the radio sources are visible or not (Make f-t diagrams)
- ③ Check the time to finish receiving radio waves (occultation start) and the time to start receiving radio waves (occultation end) for each frequency
- ④ Examine the time lag between the occultation start/end time and our expected time for each frequency
- ⑤ Calculate the average time lag for each frequency
- ⑥ Repeat ①~⑤ with changing the maximum density and scale height of the hydrostatic equilibrium plasma model
- ⑦ Examine parameter sets when the average time lag is less than 30 sec



3-1. Ganymede ionosphere result

Ganymede1 flyby Egress part (leading / dayside / Radio-type…A)

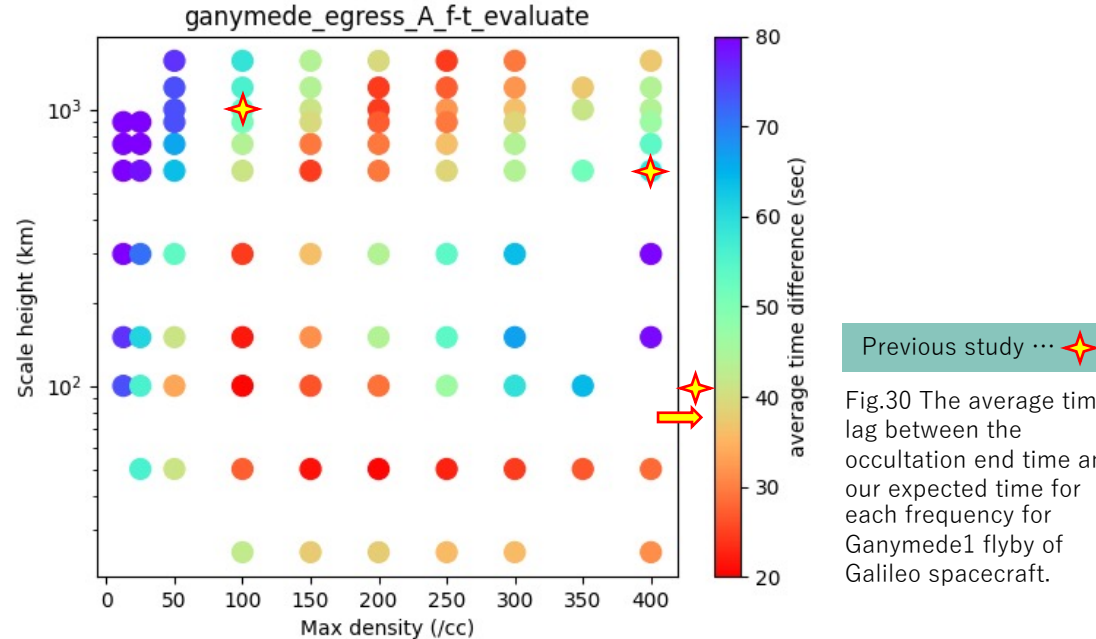
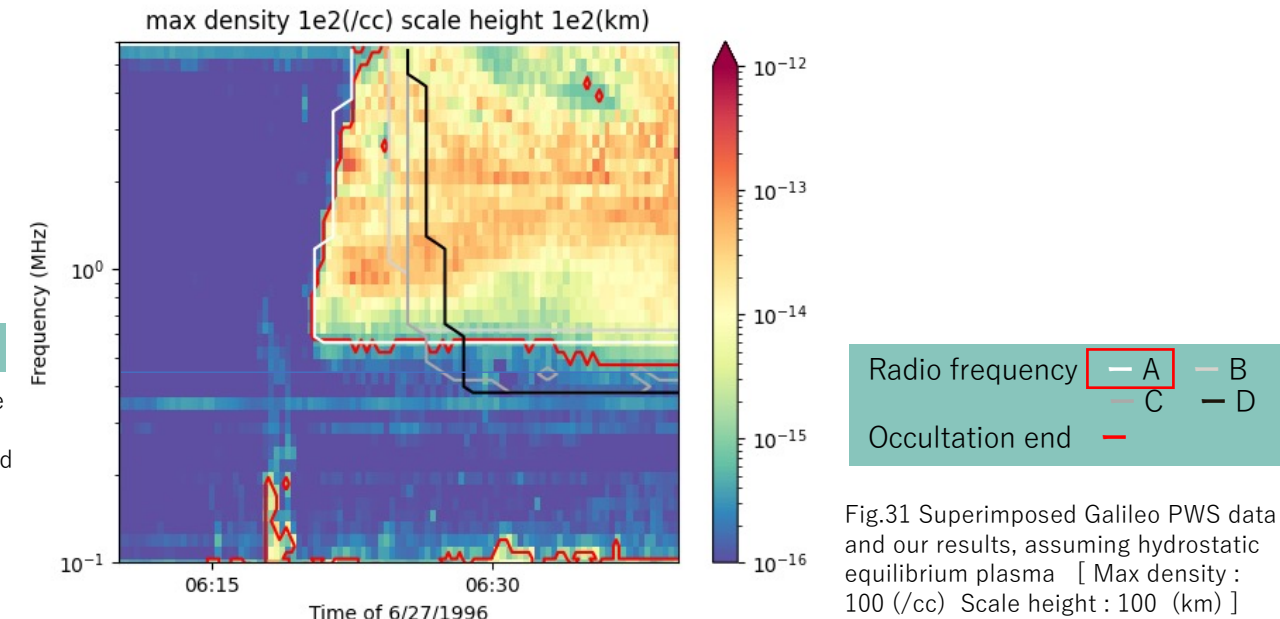


Fig.30 The average time lag between the occultation end time and our expected time for each frequency for Ganymede1 flyby of Galileo spacecraft.



Radio frequency — A — B
— C — D
Occultation end —

Fig.31 Superimposed Galileo PWS data and our results, assuming hydrostatic equilibrium plasma [Max density : 100 (/cc) Scale height : 100 (km)]

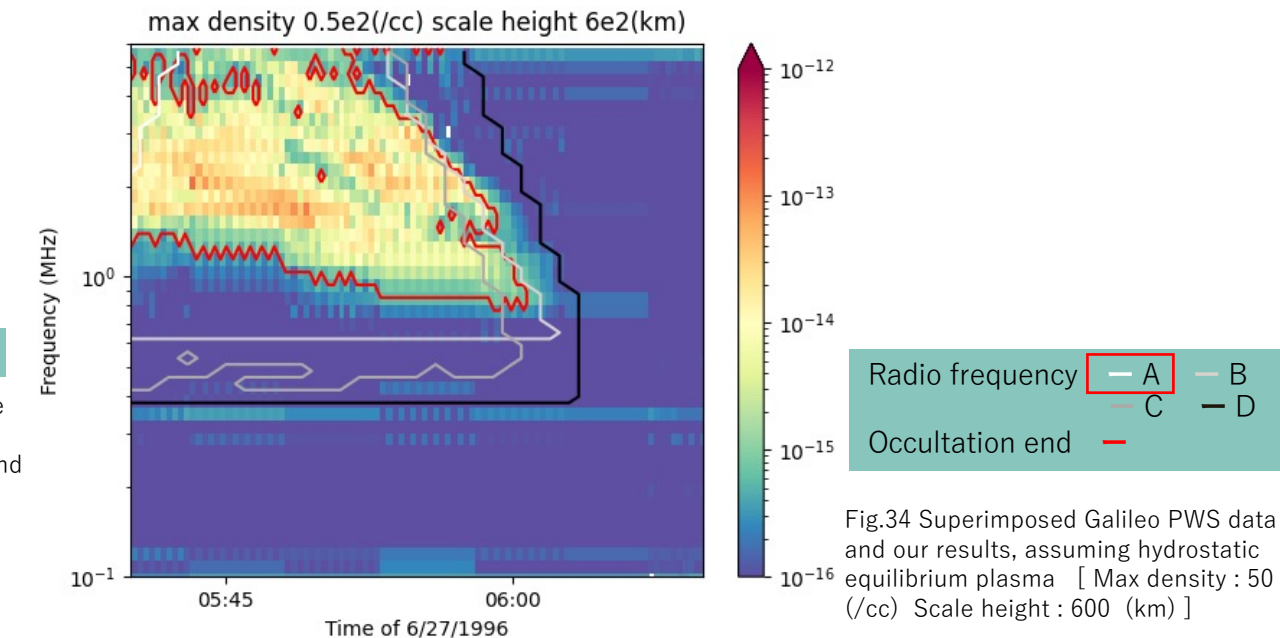
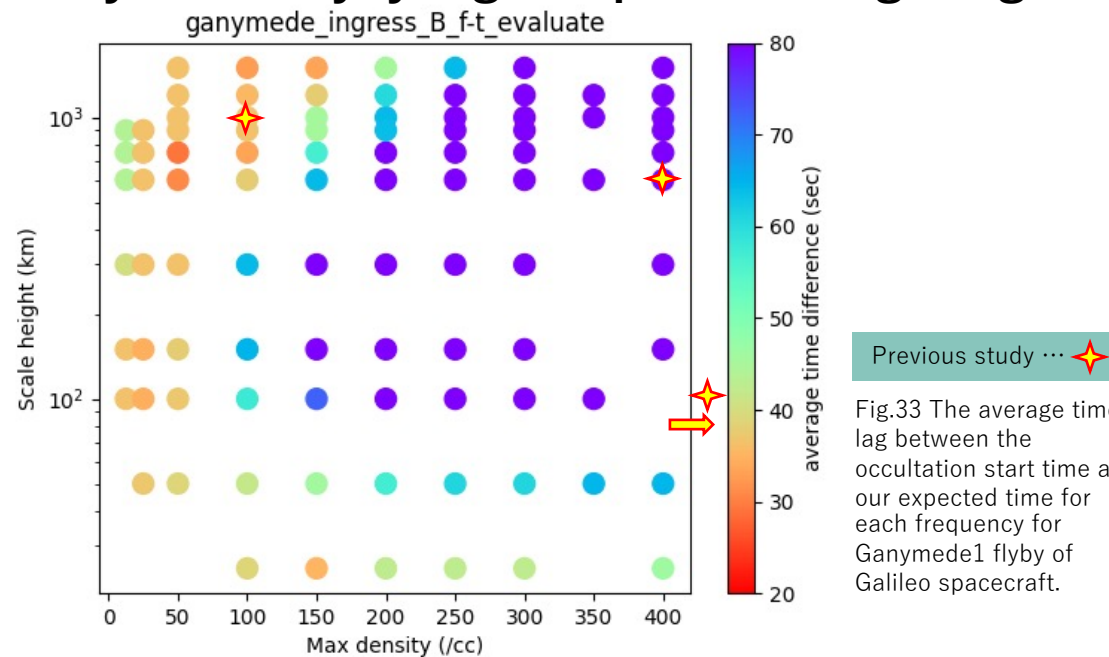
Scale height	Max density (range / best)	Cf. Previous study
1200 km	200~250 200 (/cc) (24.6 sec)	
1000 km [Gurnett et al. 1996]	200 200 (/cc) (24.6 sec)	~ 100 (/cc)
600 km [Eviatar et al. 2001a]	150~200 150 (/cc) (24.6 sec)	~ 400 (/cc)
300 km	100 100 (/cc) (24.6 sec)	
100 km [cf. Eviatar et al. 2001b]	100~200 100 (/cc) (20.6 sec)	~ 2500 (/cc)
50 km	100~ 200 (/cc) (20.6 sec)	

Max density (range) … Assuming the max density, the average time lag is less than 30 sec.
Max density (best) … Assuming the max density, the average time lag is the smallest.

Fig.32 Our results of Ganymede ionosphere max densities assuming some scale height pattern for Ganymede1 flyby egress

3-1. Ganymede ionosphere result

Ganymede1 flyby Ingress part (trailing / nightside / Radio-type...B)



Scale height	Max density (range / best)	Cf. Previous study
1200 km	- 100 (35.6 sec)	
1000 km [Gurnett et al. 1996]	- 100 (36.4 sec)	~ 100 (/cc)
600 km [Eviatar et al. 2001a]	- 50 (30.8 sec)	~ 400 (/cc)
300 km	- 50 (36.4 sec)	
100 km [cf. Eviatar et al. 2001b]	- 25 (34.6 sec)	~ 2500 (/cc)
50 km	- 25 (37.2 sec)	

Max density (range) ... Assuming the max density, the average time lag is less than 30 sec.
Max density (best) ... Assuming the max density, the average time lag is the smallest.

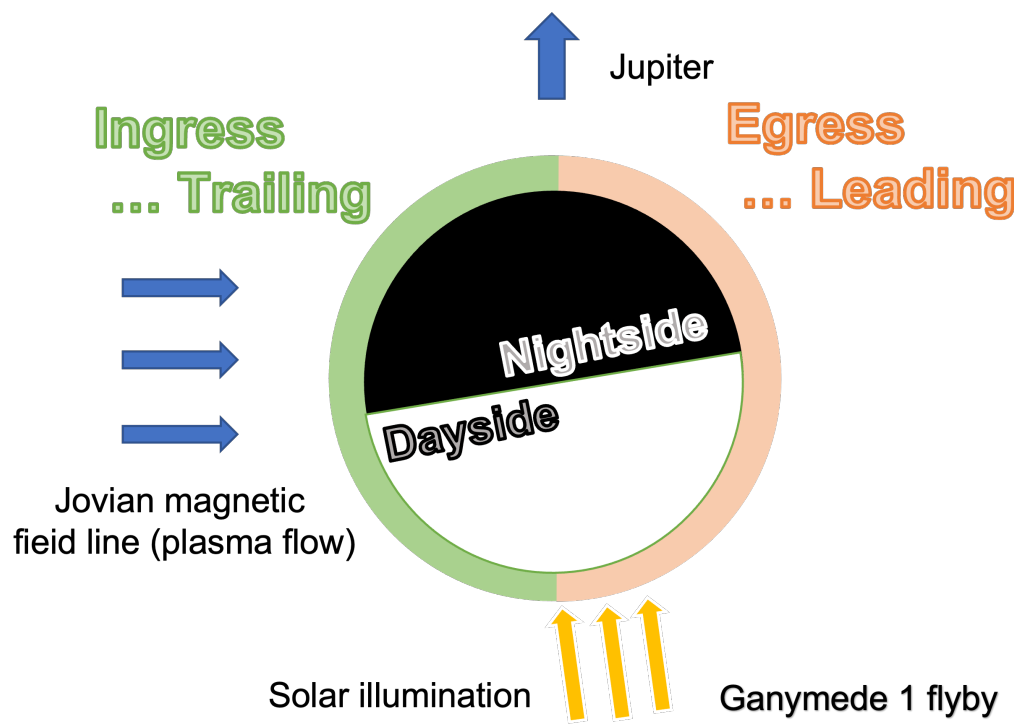
Fig.35 Our results of Ganymede ionosphere max densities assuming some scale height pattern for Ganymede1 flyby ingress

3-2. Discussion of Ganymede ionosphere results

29

Scale height	Egress max (range / best)	Ingress Max (range best)	Cf. Previous study
1000 km	200 200 (/cc) (24.6 sec)	- 100 (36.4 sec)	~ 100 (/cc)
600 km	150~200 150 (/cc) (24.6 sec)	- 50 (30.8 sec)	~ 400 (/cc)
100 km	100~ 200 (/cc) (20.6 sec)	- 25 (34.6 sec)	~ 2500 (/cc)

Fig.36 Our results of Ganymede ionosphere max densities assuming some scale height pattern for Ganymede1 flyby



Max density (range) ... Assuming the max density, the average time lag is less than 30 sec.
 Max density (best) ... Assuming the max density, the average time lag is the smallest.

- There is day-night asymmetry of ionospheric structure in our results of Ganymede.
- The existence of an ionosphere depend on solar illumination rather than the electron impact (?).
- Reconnected field lines serve the leading hemisphere plasma. (?) [[Khurana et al., 2007](#)]
- We are considering new methods for distinguish these plasma distributions. (Using Faraday rotation, radio direction, intensity and phase)

3-3. Europa ionosphere result

Europa12 flyby results 1996/07/27

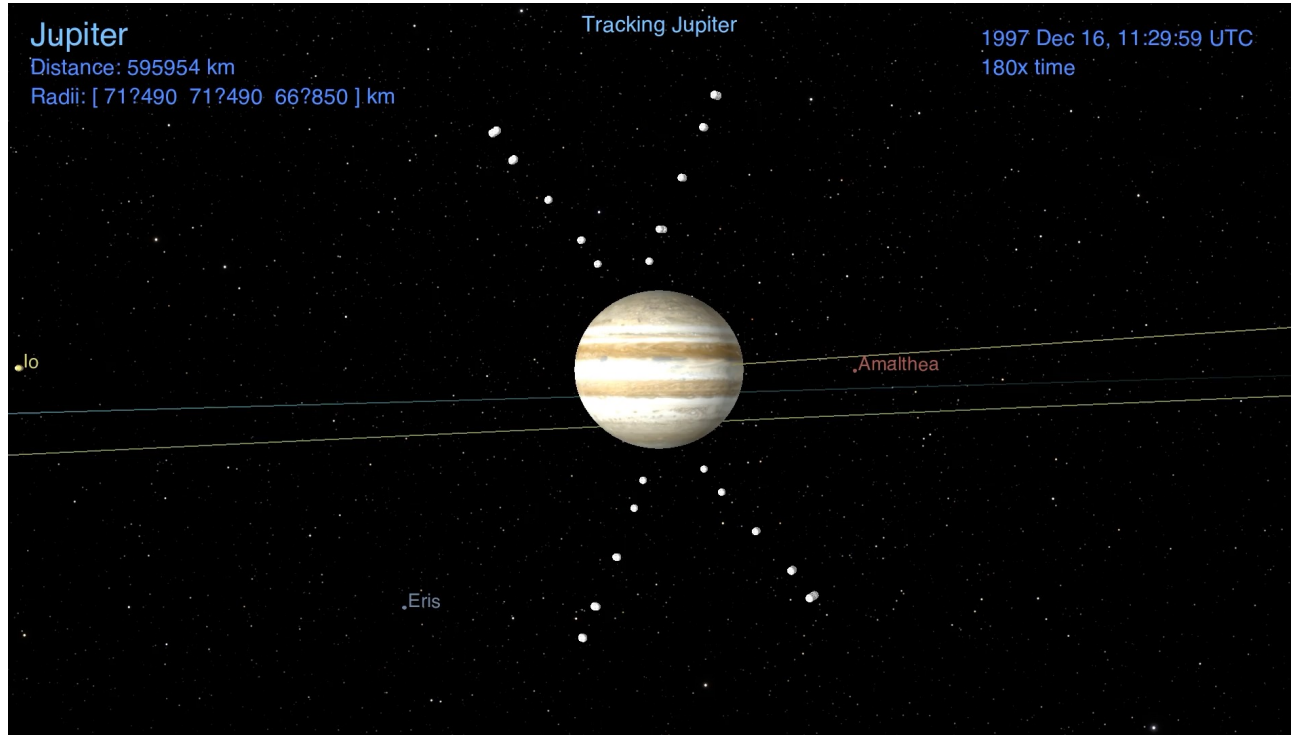


Fig.37 Flyby visualized in the Cosmographia tool. The scene is set with an observer on the Galileo spacecraft, pointing to Jupiter. Europa is in the field of view. The ExPRES-modelled visible radio sources are also shown, at 700 kHz, 1 MHz, 2 MHz, 5 MHz and 10 MHz as white dots. The radio sources are conventionally grouped in four sets (named A, B, C and D). [Cecconi et al, 2021]

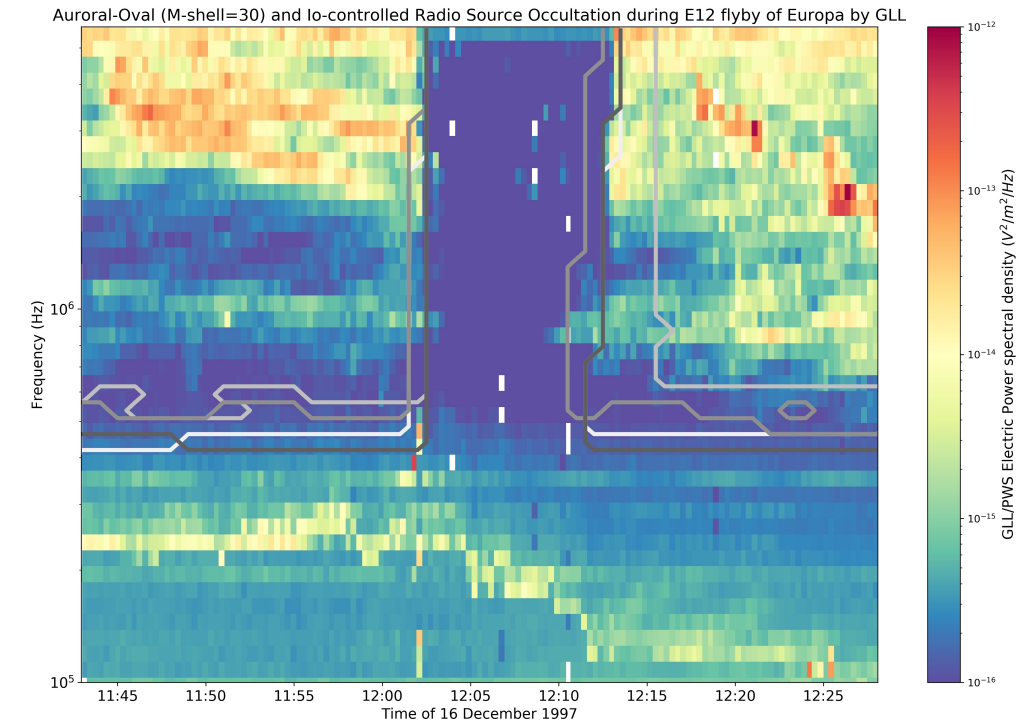


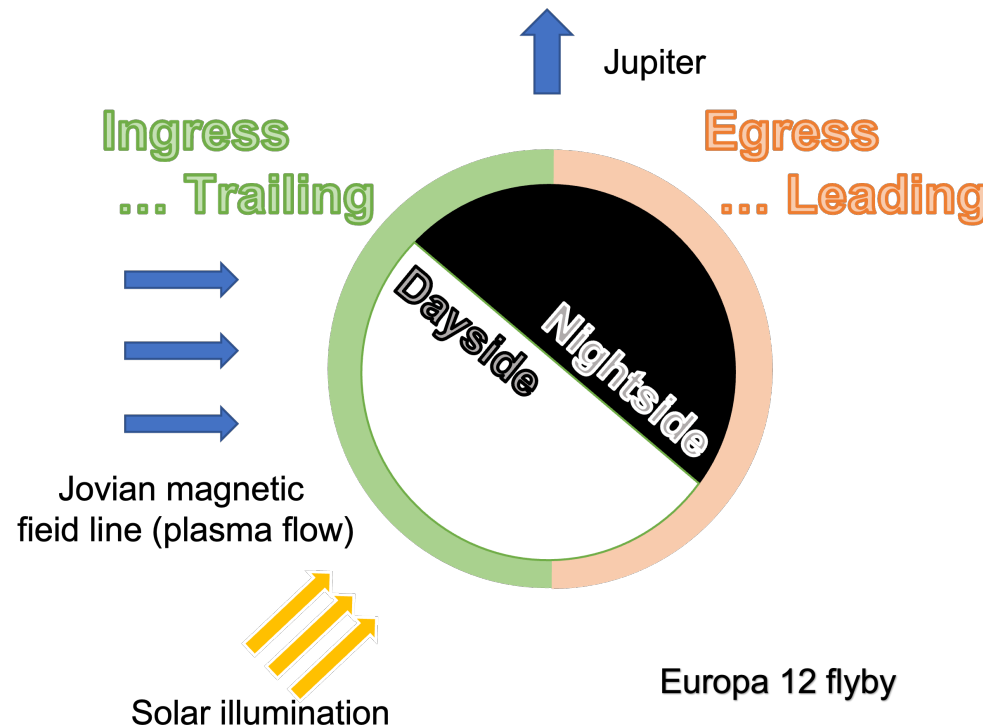
Fig.38 Superimposed Galileo PWS data and ExPRES simulations during Jovian radio emission occultations by Europa. The four types of emission (A, B, C, D) are separated (from white to darkgrey, resp.) [Cecconi et al, 2021]

3-4. Discussion of Europa ionosphere results

32

Scale height	<i>Egress max (range / best)</i>	<i>Ingress Max (range best)</i>	Cf. Previous study
900 km	$\sim 350 \mid 150 \sim 300$ (/cc) (23.9 sec)	$\sim \mid \sim$ (/cc) (28.0 sec)	Max ... 9000 ± 4000 /cc
600 km	$\sim 300 \mid 150 \cdot 200$ (/cc) (23.9 sec)	$\sim \mid \sim$ (/cc) (28.0 sec)	Scale height ... 240 ± 40 km (~ 300 km) 440 ± 60 km (300 km \sim)
300 km	$\sim 200 \mid 100 \cdot 150$ (/cc) (23.9 sec)	$\sim \mid \sim$ (/cc) (28.0 sec)	

Fig.44 Our results of Ganymede ionosphere max densities assuming some scale height pattern for Europa12 flyby



Max density (range) ... Assuming the max density, the average time lag is less than 30 sec.
Max density (best) ... Assuming the max density, the average time lag is the smallest.

- There is no clear signature of Europa ionosphere especially in ingress part.
- The observation results can be sufficiently reproduced without considering the refraction effect.
- We need a wide parameter range study to examine the upper limits of electron density.

[Background]

- Structures of the interior and ionosphere of the icy moons are essential information for understanding universality of habitable environment.

[Purpose]

- Investigate spatial structures of ionosphere created from the water oceanic materials, developing the numerical simulation code for the radar explorations using natural radio waves.

[Result & Discussion]

- There is day-night (or leading-trailing) asymmetry of ionospheric structure in our Ganymede result. (photo ionization?)
- We are considering new methods for distinguish these plasma distributions. (Using Faraday rotation, radio direction, intensity and phase)
- There is no clear signature of Europa ionosphere.
- We need a wide parameter range study to examine the upper limits of electron density.

~ For occultation ~

- ・ ガニメデ・エウロパにおける結果の議論を進める&カリストの電子密度推定
- ・ 惑星電波を用いた電離圏掩蔽観測で論文執筆 (JpGU and MOP にて結果を発表)

~ For passive Radar ~

- ・ 指定した確率で氷衛星表面で反射・透過する電波の再現 (済)
- ・ 掩蔽論文執筆後、コード開発を再開 (M2 後半でのテーマ?)

6. Reference

- Aharon Eviatar, Vytenis M. Vasyliūnas, Donald A. Gurnett (2001), The ionosphere of Ganymede, Planetary and Space Science Volume 49, Issues 3–4, March 2001, Pages 327–336
- B. Cecconi, C. K. Louis, C. Muñoz Crego, and C. Vallat (2021), Auroral Radio Source Occultation Modeling and Application to the JUICE Science Mission Planning
- Kazuo Ouchi (2017), Principles of Radar - From Search Radar to Synthetic Aperture Radar, Publisher: Corona Publishing Co.
- Kimura, T., F. Tsuchiya, H. Misawa, A. Morioka, and H. Nozawa (2008a), Occurrence and source characteristics of the high - latitude components of Jovian broadband kilometric radiation, *Planet. Space Sci.*, **56**, 1155– 1168, doi:[10.1016/j.pss.2008.03.001](https://doi.org/10.1016/j.pss.2008.03.001).
- Paterson, W. R., Frank, L. A. Ackerson, K. L (1997), Galileo plasma observations at Europa: Ion energy spectra and moments, *Journal of Geophysical Research*, Volume 104, Issue A10, p. 22779-22792, doi:10.1029/1999JA900191
- Xianzhe Jia, Margaret G. Kivelson, Krishan K. Khurana and William S. Kurth (2018), Evidence of a plume on Europa from Galileo magnetic and plasma wave signatures, *Nature Astronomy* 2, 459–464 (2018),
- Kliore, A. J., Anabtawi, A. Nagy, A. F.; Galileo Radio Propagation Science Team (2001), The ionospheres of Ganymede and Callisto from Galileo radio occultations, *Bulletin of the American Astronomical Society*, Vol. 33, p.1084 DOI: 10.1038/s41550-018-0450-z
- M. A. McGrath, C. J. Hansen, A. R. Hendrix, Kurt Retherford (2009), Observations of Europa's Tenuous Atmosphere, *Europa*.
- MASER HP <https://maser.lesia.obspm.fr/publications/doi/auroral-radio-source-occultation.html?lang=en#G01> (2021/5/2)
- NASA HP <https://www.nasa.gov/topics/solarsystem/features/pia16826.html> (2021/5/2)
- GCOE HP <https://www.gcoe-earths.org/en/jupiter.html> (2021/5/2)
- McGrath, Melissa A.; Lellouch, Emmanuel; Strobel, Darrell F.; Feldman, Paul D.; Johnson, Robert E. (2004), Satellite atmospheres, *Jupiter*
- Hartkorn, Oliver, 2017. Modeling Callisto's Ionosphere, Airglow and Magnetic Field Environment. Technical Report. Köln Universitat.
- Khurana, K., Kivelson, M., Stevenson, D. *et al.* Induced magnetic fields as evidence for subsurface oceans in Europa and Callisto. *Nature* 395, 777–780 (1998).
- M.G. Kivelson, K.K. Khurana, M. Volwerk (2002), The permanent and inductive magnetic moments of Ganymede, *Icarus*, 157, pp. 507–522
- Schubert et al. (2004). Interior, composition, structure and dynamics of the Galilean satellites, in *Jupiter. The planet, satellites and magnetosphere*, Cambridge University Press
- D.A. Gurnett, W. S. Kurth, A. Roux, S.J. Bolton & C.F. Kernel (1996), Evidence for a Magnetosphere at Ganymede from Plasma-wave Observations by the Galileo Spacecraft. *Nature* 384(6609) doi: 10.1038/384535a0
- Eviatar, A., Vasyliūnas, M. V., & Gurnett, A. D. (2001a). The ionosphere of Ganymede. *Planetary and Space Science*, 49(3), 327–336. <https://doi.org/10.1016/S0032-0633%2800%2900154-9>
- Aharon Eviatar, Darrell F. Strobel, Brian C. Wolven, Paul D. Feldman, Melissa A. McGrath, and Donald J. Williams (2001b), Excitation of the Ganymede Ultraviolet Aurora. *THE ASTROPHYSICAL JOURNAL*, 555 : 1013È1019, 2001 July 10
- G. Carnielli, M. Galand, F. Leblanc, L. Leclercq, R. Modolo, A. Beth, H.L.F. Huybrighs, X. Jia (2019), First 3D test particle model of Ganymede's ionosphere, *Icarus* Volume 330, 15 September 2019, Pages 42–59 <https://doi.org/10.1016/j.icarus.2019.04.016>
- A. J. Kliore, A. Anabtawi, R. G. Herrera, S. W. Asmar, A. F. Nagy, D. P. Hinson, and F. M. Flasar (2002), Ionosphere of Callisto from Galileo radio occultation observations, *JOURNAL OF GEOPHYSICAL RESEARCH*, VOL. 107, NO. A11, 1407, doi:10.1029/2002JA009365, 2002
- D. A. Gurnett, A.M. Persoon, W. S. Kurth (2000), Plasma densities in the vicinity of Callisto from Galileo plasma wave observations, *GEOPHYSICAL RESEARCH LETTERS*, VOL. 27, NO. 13, PAGES 1867–1870, JULY 1, 2000
- D. A. Gurnett, W. S. Kurth, A Rouxt & S. J. Bolton (1997), Absence of a magnetic-field signature in plasma-wave observations at Callisto, *NATURE* | VOL 387 | 15 MAY 1997
- A. J. Kliore, D. P. Hinson, F. M. Flasar, A. F. Nagy, T. E. Cravens (1997), The Ionosphere of Europa from Galileo Radio Occultations, *Science* 18 Jul 1997: Vol. 277, Issue 5324, pp. 355–358 DOI: 10.1126/science.277.5324.355
- Kliore, A. J.; Anabtawi, A.; Nagy, A. F (2001), The Ionospheres of Europa, Ganymede, and Callisto American Geophysical Union, Fall Meeting 2001, abstract id.P12B-0506
- W.S. Kurth; D.A. Gurnett, A.M. Persoon, A. Roux, S.J. Bolton, C.J. Alexander (2001), The plasma wave environment of Europa, *Planetary and Space Science* 49 (2001) 345–363

Appleton-Hartree equation

~The dispersion relation of waves in magnetized cold plasma~

$$D(t, \vec{r}, \omega, \vec{k}) = \left(\frac{c|\vec{k}|}{\omega}\right)^2 + \frac{2X}{2 - \frac{Y^2 \sin^2 \theta}{1-X} + \rho \sqrt{\frac{Y^2 \sin^4 \theta}{(1-X)^2} + 4Y^2 \cos^2 \theta}} - 1 = 0 \quad \cdots (1)$$

$$X = \left(\frac{\omega_p}{\omega}\right)^2 \quad Y = \frac{\omega_c}{\omega} \quad \rho = \begin{cases} 1 & \text{LO mode} \\ -1 & \text{RX mode} \end{cases}$$

\vec{r}, t : position of a ray path and time

θ : an angle between wave normal vector and the local magnetic field vector

ω_p : plasma frequency (depending on plasma density)

ω_c : cyclotron frequency (depending on magnetic field)

- Derived from the equation of motion for plasma and Maxwell's equation

(Cold plasma · Discarding plasma collision)

- Under the Eq-(1) condition, electromagnetic wave in plasma can exist.
- Trace the ray propagation meeting this condition.

... Raytracing

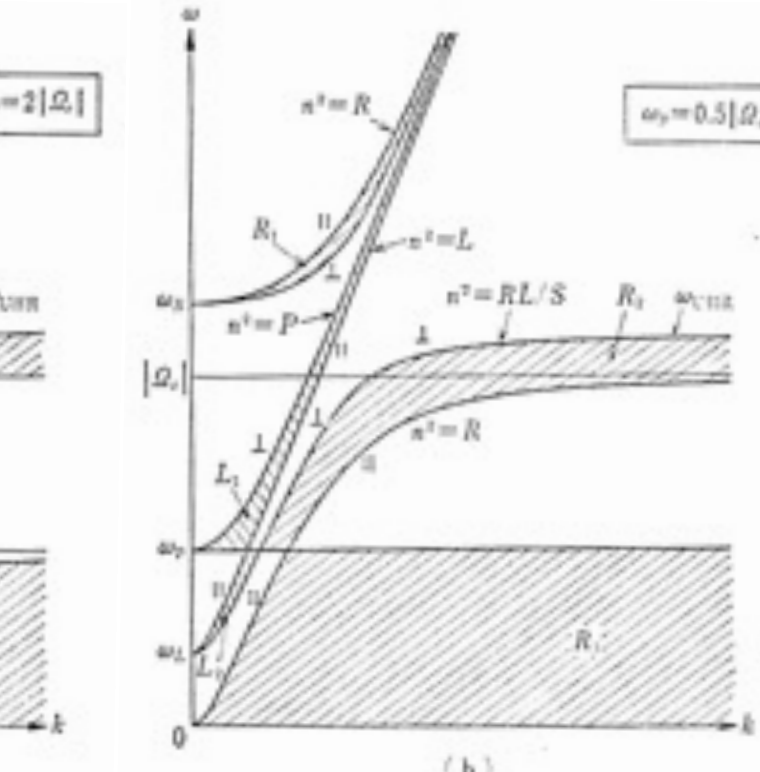
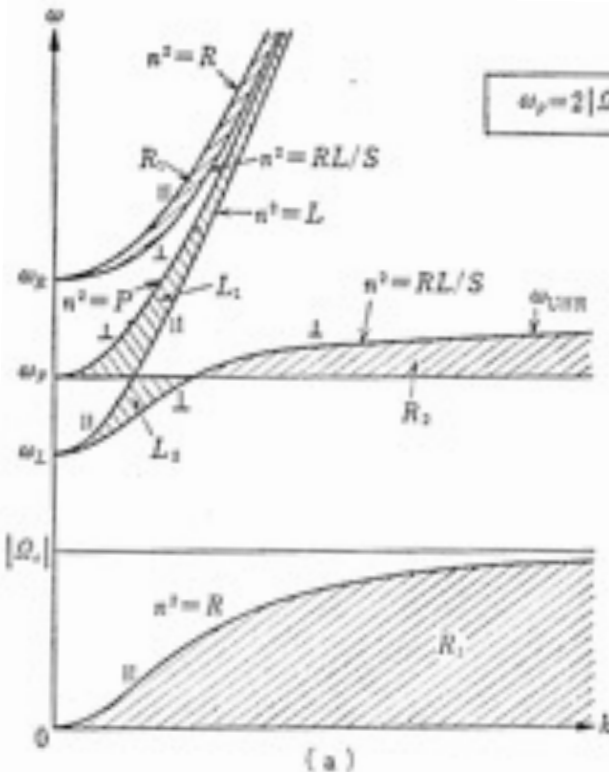


Fig.16 $\omega - k$ diagram ($\omega_p = 2|\Omega_e|, \omega_p = 0.5|\Omega_e|$) ["Gendai Denjihadouron"]

6. B - ExPRES code

[Hess et al., 2008]

ExPRES code

- ・観測者的位置に伝わってくる電波が時間ごとにどのようなスペクトルをもつかモデリングするシミュレーションコード

～フリーパラメータ～

- ・ある時刻における観測者・イオ・木星の位置関係
- ・リード角 δ …電波源となる磁力線とイオを貫く磁力線の経度差
- ・磁場モデル
- ・電子の速度分布の種類→ビーム角 θ の指定
 - …ロスコーンタイプの場合 40-80° 程度
ロスコーン角の大きさで決定
 - …シェルタイプの場合 90°(const)付近
- ・ビーム角の厚み $\delta\theta$

(直進波を仮定)

時間ごとに観測される周波数を
周波数 - 時間平面で表示

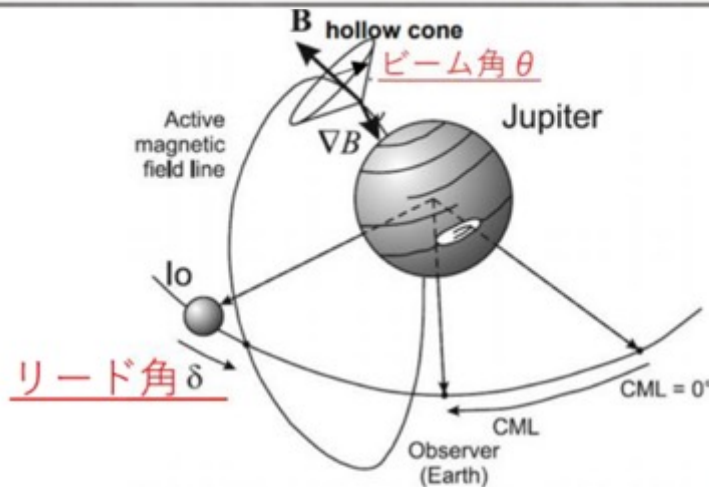


Fig.18 パラメータの位置関係 [Galopeau et al. 2007]

電波源との位置関係
と周波数が決定

電波放射の
向きと幅が決定

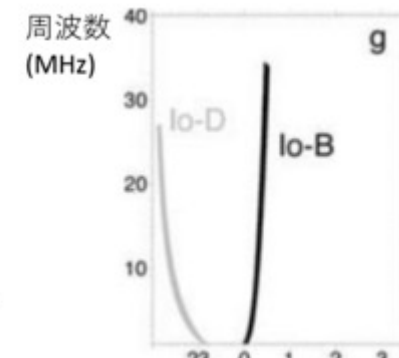


Fig.19 シミュレーション結果の一例 [Hess et al., 2008]

CMI (サイクロトロンメーザー不安定)

- ①磁力線周りに旋回しながら伝搬する電波と電子が同じ周期
(もしくはその整数倍で) で振動する (共鳴条件)
- ②プラズマ物理の理論から計算される電波の成長率が有意に大きい

①と②の条件により

→電子の磁力線水平・垂直方向の速度に対する分布「速度分布関数」の形状によって
成長率が最大となるビーム角 θ が定まる

電波の成長を引き起こす代表的な二つの速度分布関数の有力候補

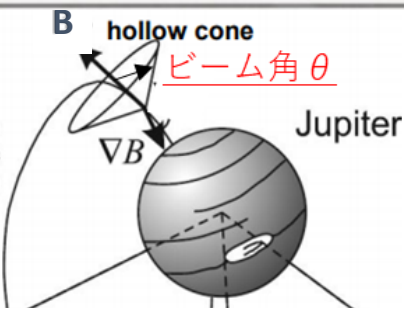
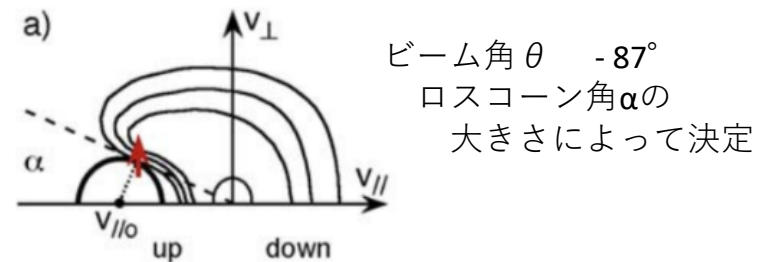


Fig.18 パラメータの位置関係
[Galopeau et al. 2007]

a) 口スコーンタイプ
‥電子の全方向へのランダムな加速



b) シェルタイプ
‥電子の v_{\parallel} 方向のモノリシックな加速

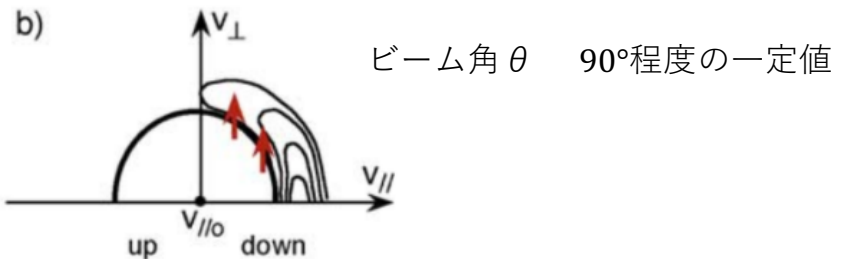


Fig.19 各タイプの電子の速度分布関数[Hess et al., 2008]

測度分布関数の解明 → 加速過程の解明

木星探査機Juno/Waves による波動観測結果との比較 [Louis et al., 2017]

- ・モデルとの比較による観測された電波源の位置（北or南半球）の識別
- ・Junoの周回衛星ならではの広い緯度域からの新たにパラメータの制約が可能に
→より正確にCMIによる電波放射の観測を再現するシミュレーションに成功
→電子・イオンの直接観測と比較

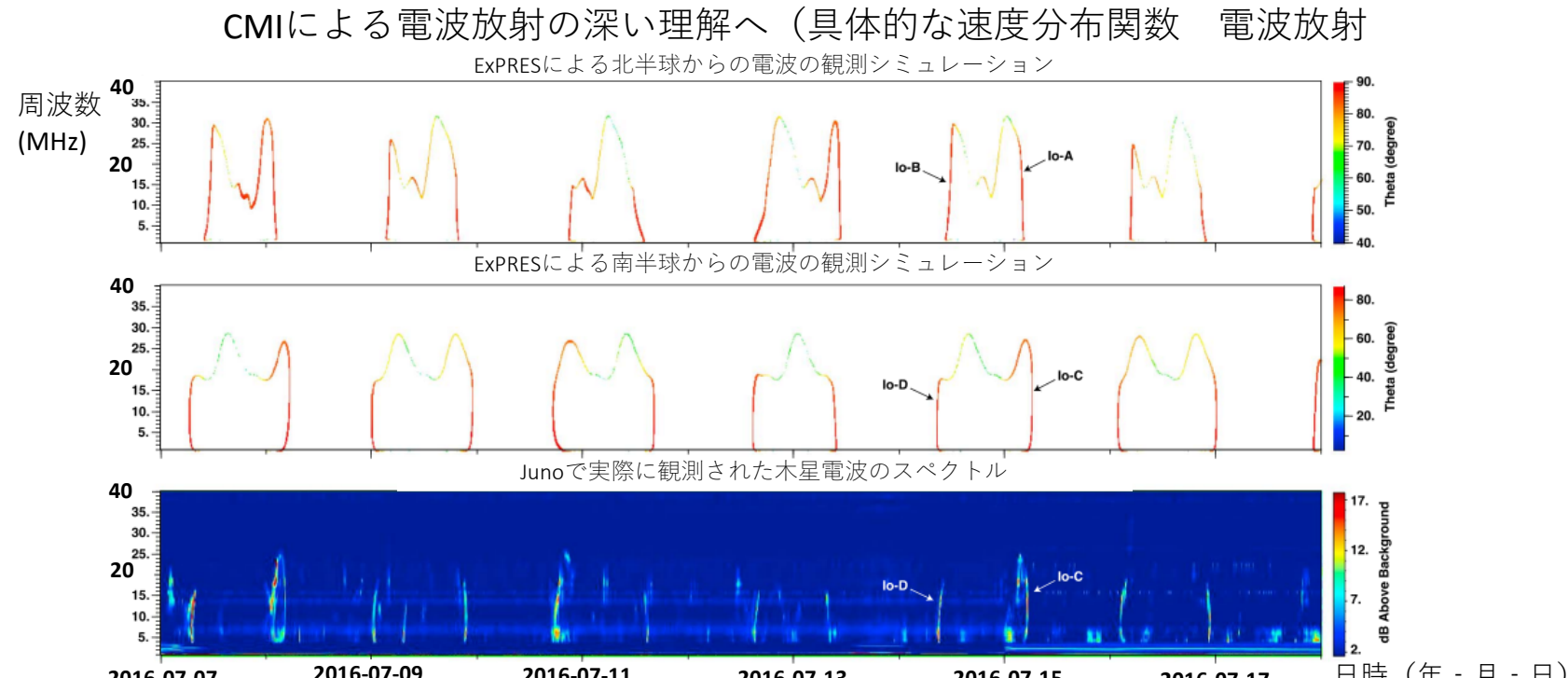


Fig.20 下から Junoで観測された木星電波のスペクトル、ExPRESによる南半球からの電波の観測シミュレーション
ExPRESによる北半球からの電波の観測シミュレーション [Louis et al., 2017a]

速度分布関数のタイプから発生する放射角の導出方法

- ①伝搬している電波と電子が同じ周期（もしくはその整数倍で）で振動する（共鳴条件）

$$\text{共鳴条件} \cdots \omega = \frac{\omega_{CE}}{\Gamma} + k_{\parallel} v_{\parallel}$$

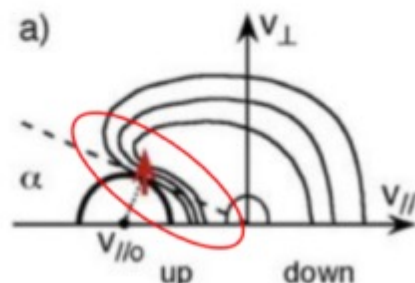
$\rightarrow v_{\parallel 0} \sim c \cos \theta$ を中心とした速度平面上の円にある電子が電波法射

- ②プラズマ物理の理論から計算される共鳴による電波の成長率が有意に大きい

$$\text{電波の成長率} \cdots \gamma \propto \int_{R.C.} v_{\perp}^2 \nabla v_{\perp} f(v) dv \quad (\text{積分経路} \cdots \text{共鳴条件の速度平面上の円})$$

$\rightarrow \nabla v_{\perp} f(v) > 0$ となるような積分経路を持つ円での放射大

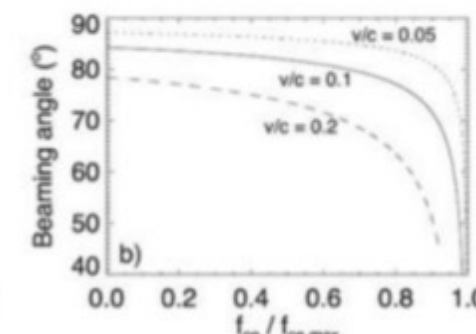
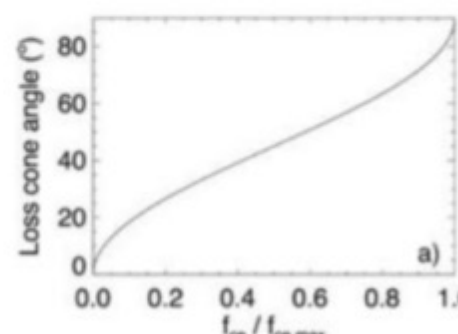
a) ロスコーンタイプ



$$v_{\parallel 0} = v / \cos \alpha = v / \left(1 - \frac{\omega_{ce}}{\omega_{ce,max}}\right)^{1/2}$$

$$\rightarrow \theta = \arccos \left[(v/c) / \left(1 - \omega_{ce}/\omega_{ce,max}\right)^{1/2} \right]$$

ビーム角 θ 鋭角(40-80° 程度)
ロスコーン角 α の大きさで決定



JUICE RPWI – HF – RWI preamp : Required Spec.s

- Developed by Tohoku Univ.(Jpn), Meisei Elec.(Jpn) & Astronika (Pol) since 2010
- Required specifications:

Item	Required spec.	Comments
Frequency	80KHz ~ 45MHz	Fully covering Jupiter's LF – HF radio emissions (KOM – DAM)
Temperature	-180 ~ +100degC (storage) > -150degC* (operation)	Ganymede (shade) ~ Venus orbit *on PCB
Radiation dose	100krad with t=10mm Al (operation)	in Jupiter's inner magnetosphere
Gain	> 10dB	Compensation of connection loss between Antenna and RWI keeping low noise level
Noise level	< 4×10^{-20} W/m ² /Hz (4nV/m/ $\sqrt{\text{Hz}}$) @1MHz → <10nV/ $\sqrt{\text{Hz}}$ @L=2.5m	Below Galactic noise @1MHz
Dynamic range	5μV/m/ $\sqrt{\text{Hz}}$ ~ 4nV/m/ $\sqrt{\text{Hz}}$ → >52dB	Fully covering Jupiter's LF – HF radio emissions (KOM – DAM) on Jupiter's orbit (Max. signal level is near Europa.)
Ch–Ch Phase diff.	(<1deg)	On-flight calibration will be made.
Power consumption	~430mW (w/o heater) ~800mW (with heater)	Requirement from power-management

6. G – Raytracing code

Ray tracing [Kimura et al, 2008a, b, 2010 etc..] (Cf. Appendix G&H)

~ input parameter ~

- Magnetic field model $\omega_c(\vec{r}, t)$
- Plasma density model $\omega_p(\vec{r}, t)$
- Frequency of wave (ω)
- Initial position (\vec{r}_0)
- Initial wave vector (\vec{k}_0)



$d\vec{r}_{j+1}$ and $d\vec{k}_{j+1}$ in dt_j

$$(1) \rightarrow d\vec{r}_{j+1} = -\frac{\partial D_j / \partial \vec{k}_j}{\partial D_j / \partial \omega} \cdot dt_j, \quad d\vec{k}_{j+1} = +\frac{\partial D_j / \partial \vec{r}_j}{\partial D_j / \partial \omega} \cdot dt_j$$



the time (t_{j+1}), position (\vec{r}_{j+1}) and wave vector (\vec{k}_{j+1}) after dt_j

- $t_{j+1} = t_j + dt_j$
- $\vec{r}_{j+1} = \vec{r}_j + d\vec{r}_{j+1}$
- $\vec{k}_{j+1} = \vec{k}_j + d\vec{k}_{j+1}$



~ output ~

a full ray path and time ($\vec{r}(t)$)

- Equation of motion of plasma

$$\frac{d\vec{v}}{dx} = \frac{q}{m} (\vec{E} + \vec{v} \times \vec{B})$$

- Maxwell's equations

$$\nabla \times \vec{H} = \vec{j} + \frac{\partial \vec{D}}{\partial t} \quad \nabla \times \vec{E} = -\frac{\partial \vec{B}}{\partial t}$$



(Cold plasma • Discarding plasma collision)

Appleton-Hartree equation (Cf. Appendix A)

~The dispersion relation of waves in magnetized cold plasma~

$$D(t, \vec{r}, \omega, \vec{k}) = \left(\frac{c|\vec{k}|}{\omega} \right)^2 + \frac{2X}{2 - \frac{Y^2 \sin^2 \theta}{1-X} + \rho \sqrt{\frac{Y^2 \sin^4 \theta}{(1-X)^2} + 4Y^2 \cos^2 \theta}} - 1 = 0 \quad \dots (1)$$

$$X = \left(\frac{\omega_p}{\omega} \right)^2 \quad Y = \frac{\omega_c}{\omega} \quad \rho = \text{LO mode : 1, RX mode : -1}$$

\vec{r}, t : position of a ray path and time

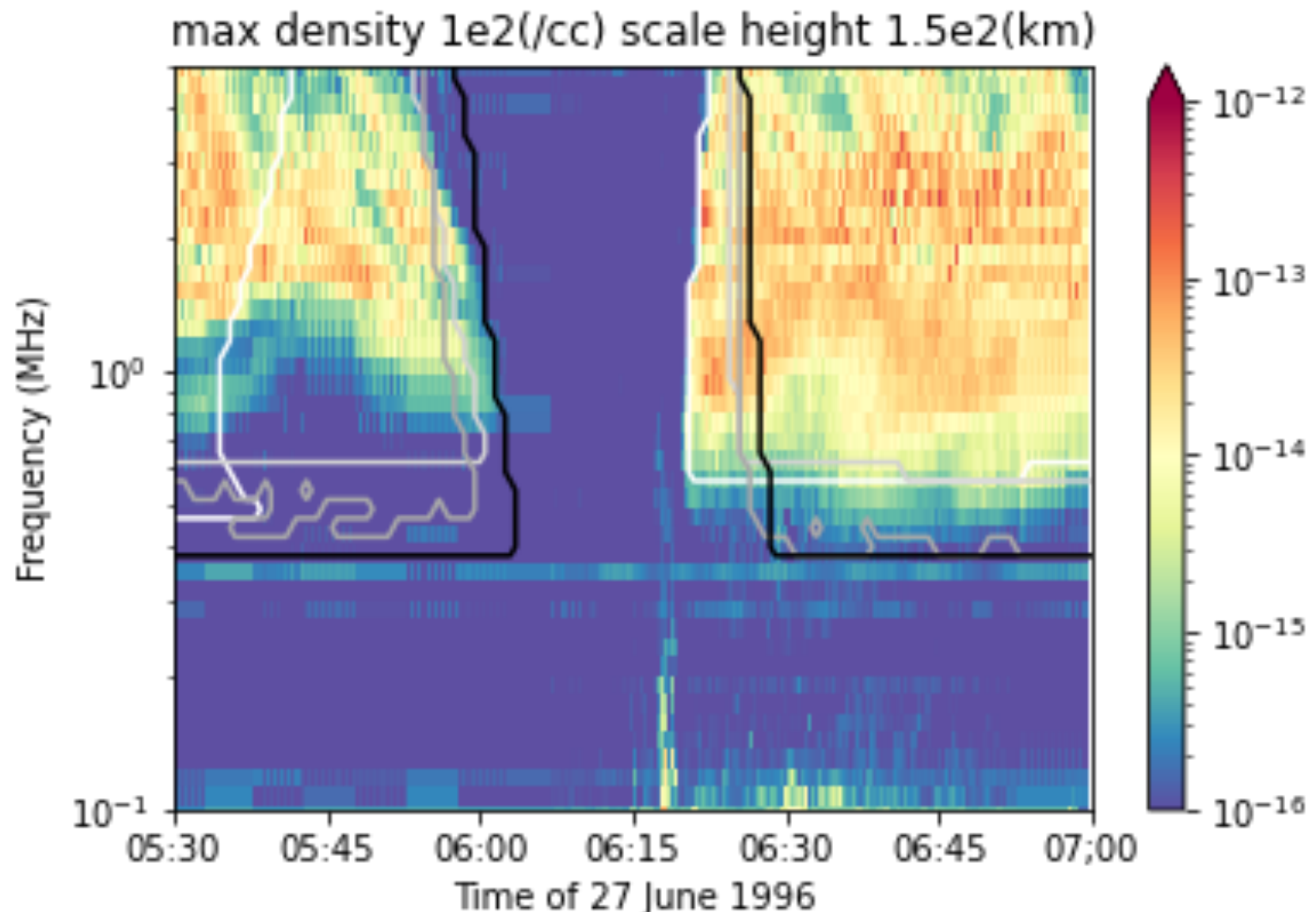
θ : an angle between wave normal vector and the local magnetic field vector

ω_p : plasma frequency (depending on plasma density)

ω_c : cyclotron frequency (depending on magnetic field)

6.H - Europa PWS result

45



6.I - Future works for passive radar

46

[For passive radar]

- We are going to simulate reflection and transmission of the EM waves in the ice crust and underlying ocean to explore their structures.
- Now I have already added reflective function on Europa's surface (Fig.22) and setting reflectance function (Fig.23).

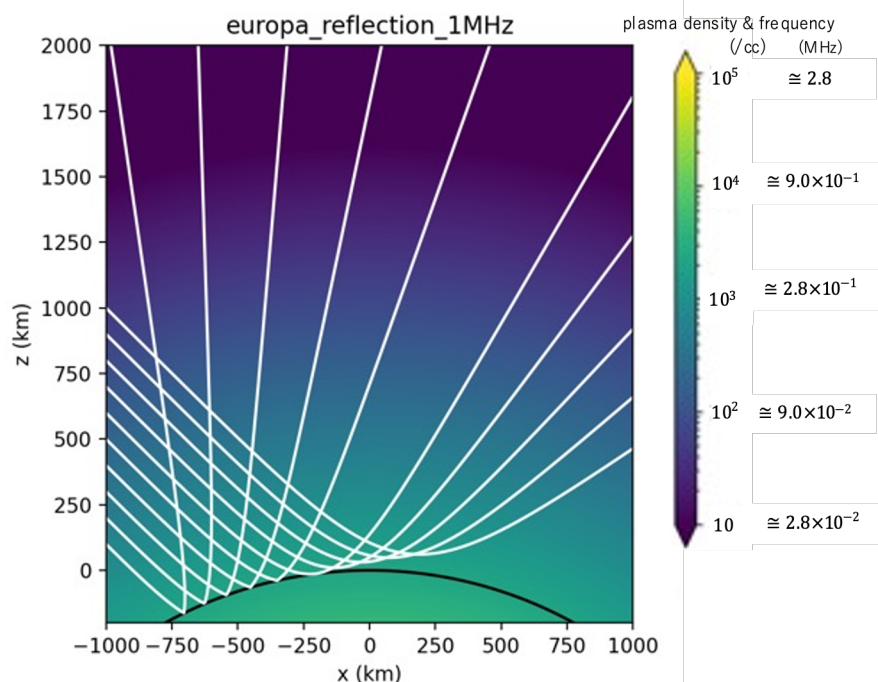


Fig.22 Surface reflection model of Europa

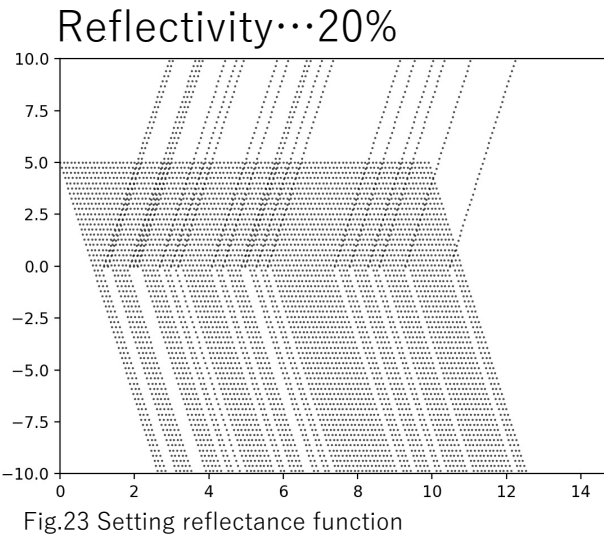
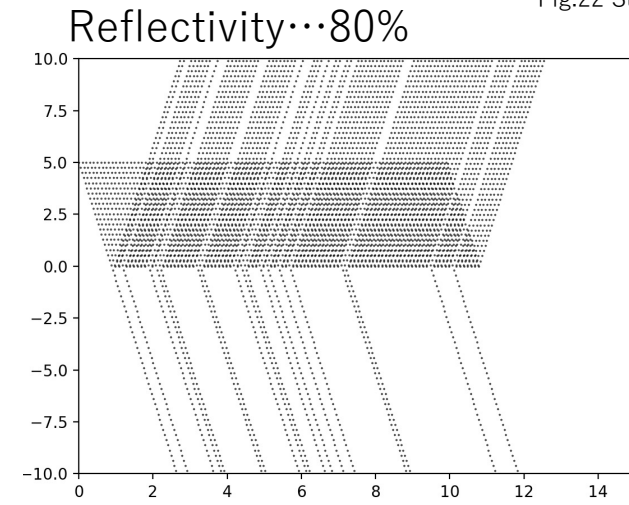
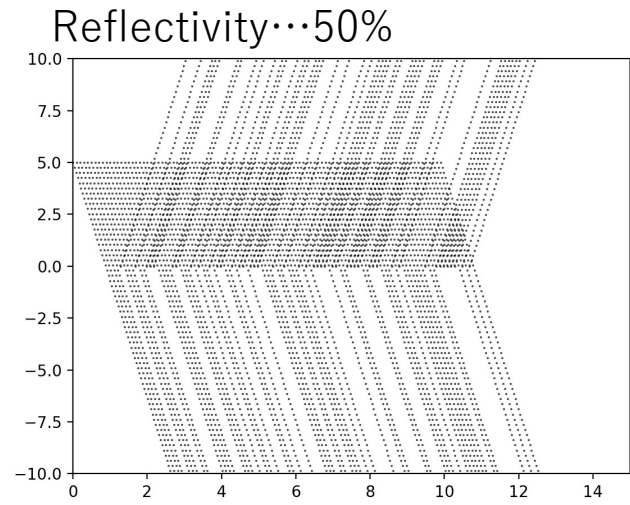


Fig.23 Setting reflectance function



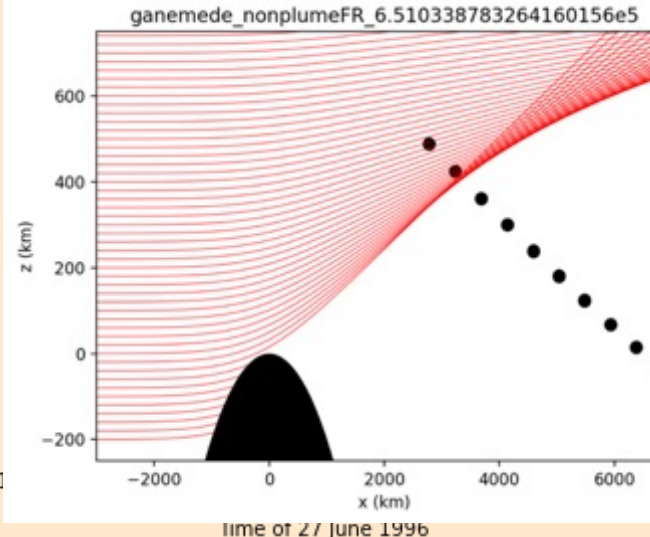
6.K –Why we can not distinguish?

47

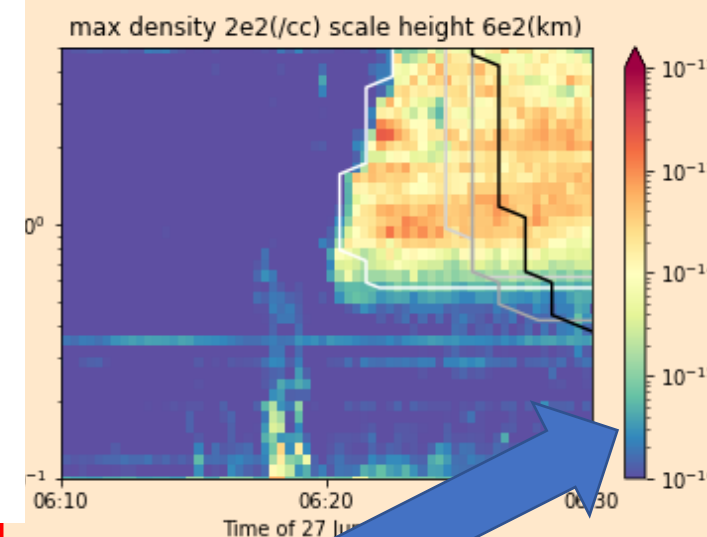
Refraction

Scale height

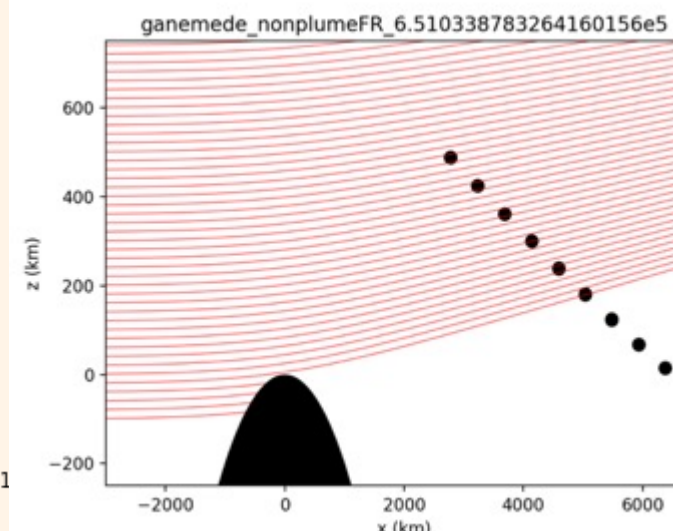
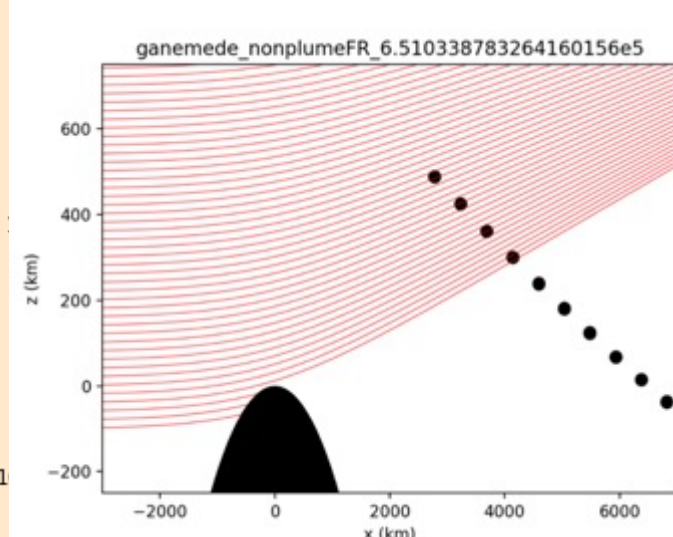
300 km



600 km

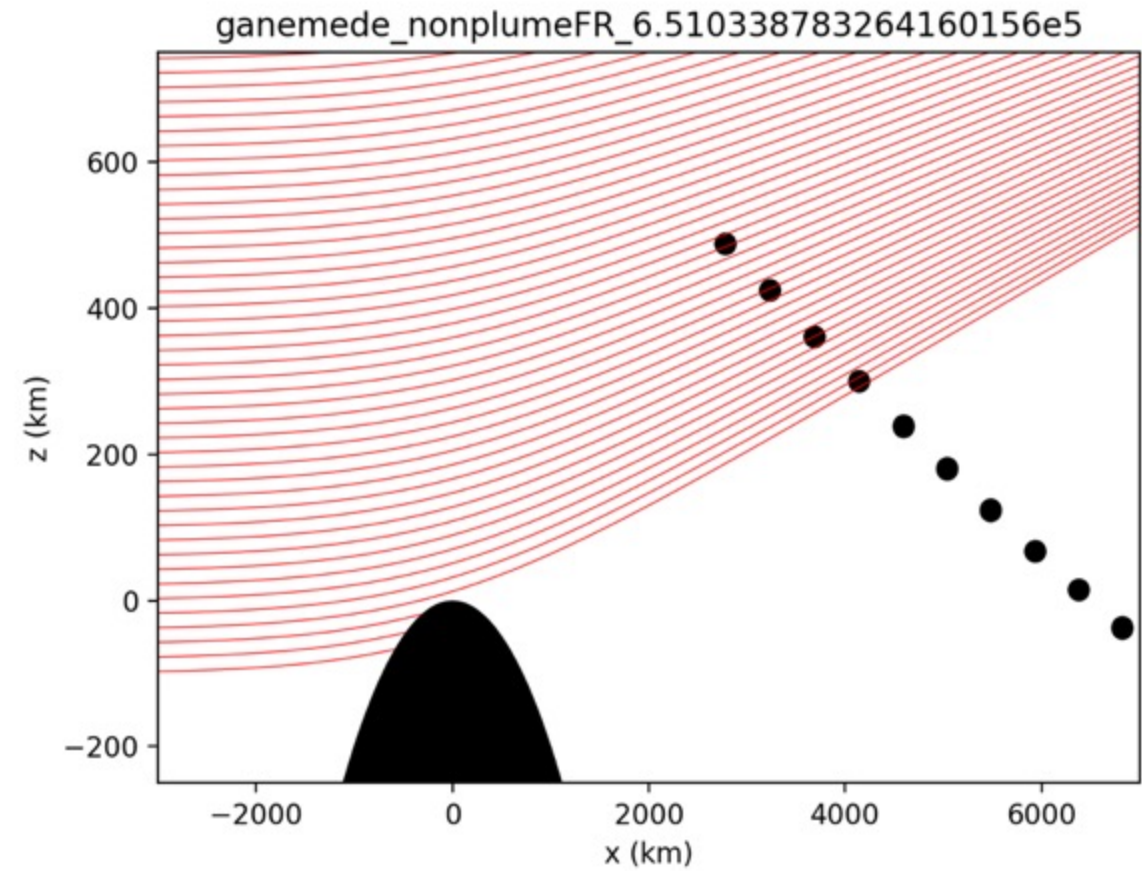
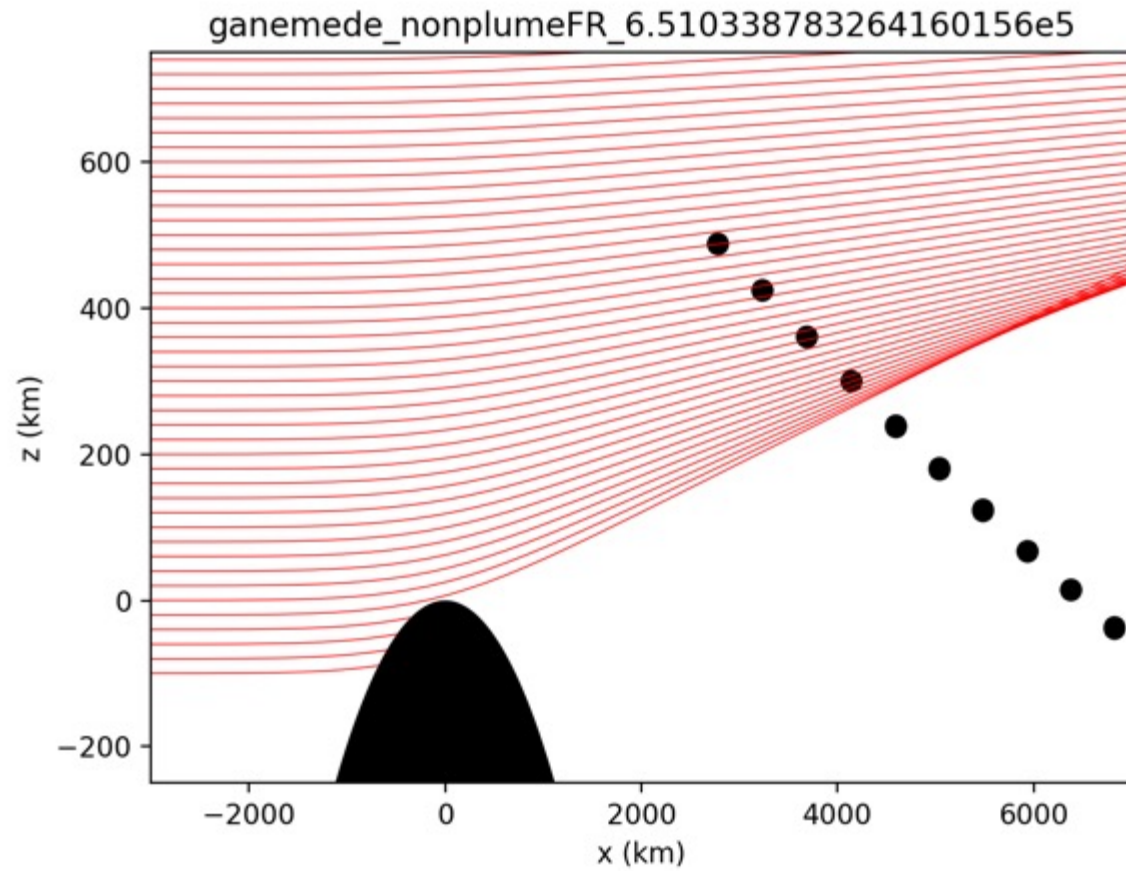


900 km



6.K –Why we can not distinguish?

48



6.L – Galileo Europa 12 flyby

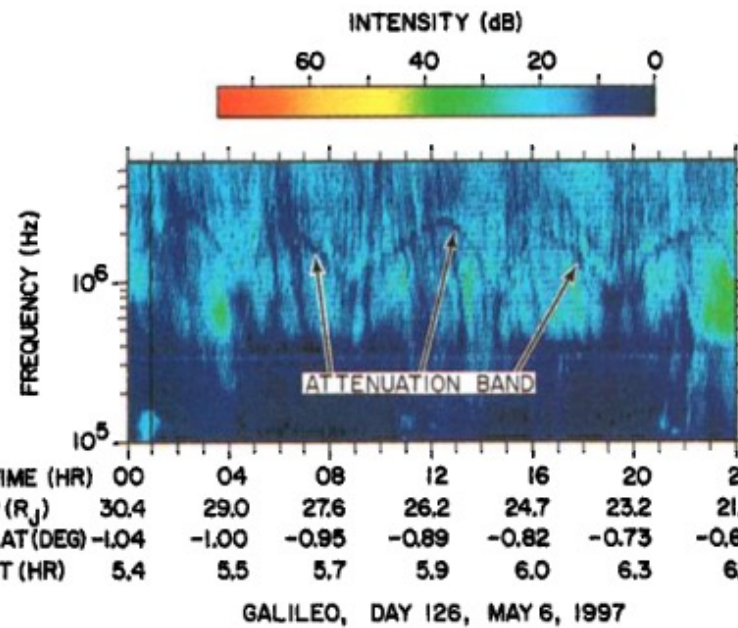


Figure 1. A frequency-time spectrogram showing the attenuation band observed in the Jovian hectometric radio emission spectrum.

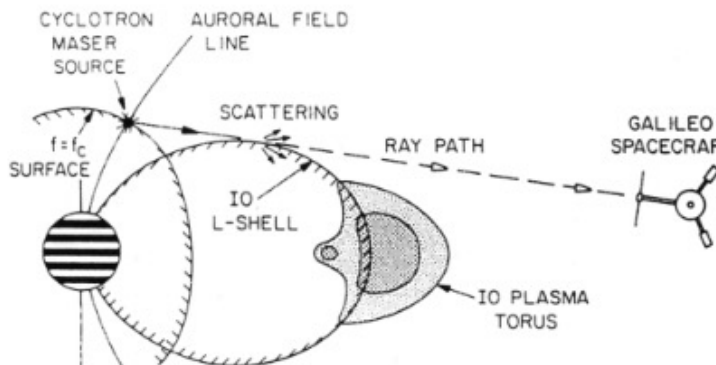
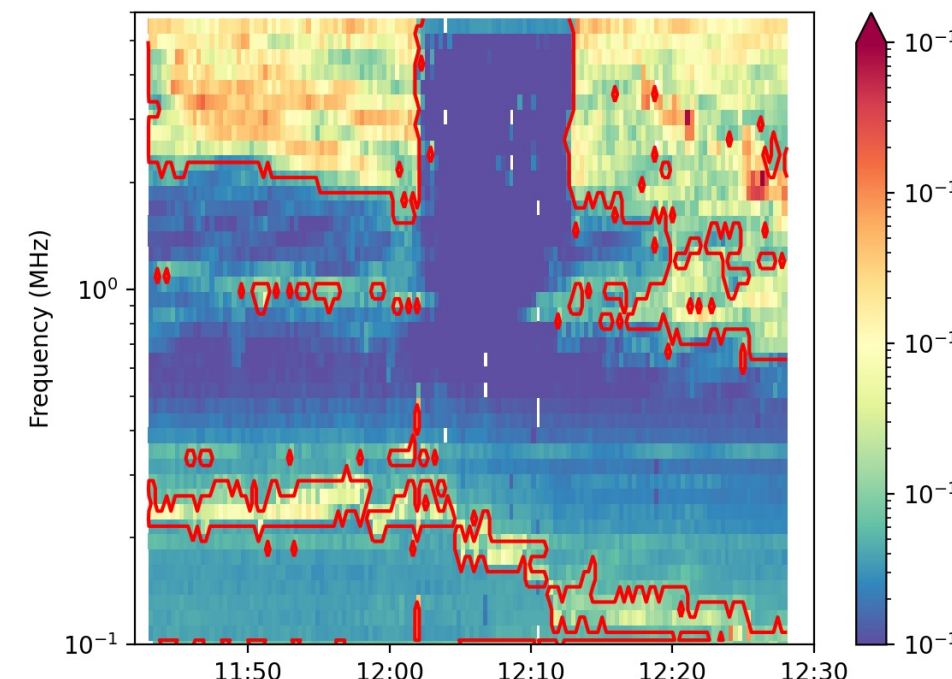


Figure 3. A model that attributes the attenuation to scattering or shallow-angle reflections in the region where the ray path is tangent to the Io L-shell.

the so-called “attenuation lanes” (Gurnett et al., 1998) resulting from the propagation of hectometric waves through the Io plasma torus (Menietti et al., 2003). The attenuation lanes are observed as a narrow-band attenuation feature modulated at the planetary rotation period. The attenuation is also accompanied or replaced with an intensification of the signal, similar to caustic optical phenomena.

The attenuation lane feature is observed at and below ~ 2 MHz before ingress, with a corresponding feature after egress, up to $\sim 12:20$. At about ~ 1 MHz, an intensification is also observed, before ingress and after egress (corresponding to the aforementioned prediction mismatch), and is probably linked to the attenuation lanes



時間分解能上げれば高周波数
いけるかも JUICEに向けて
周波数固定で位相と向き

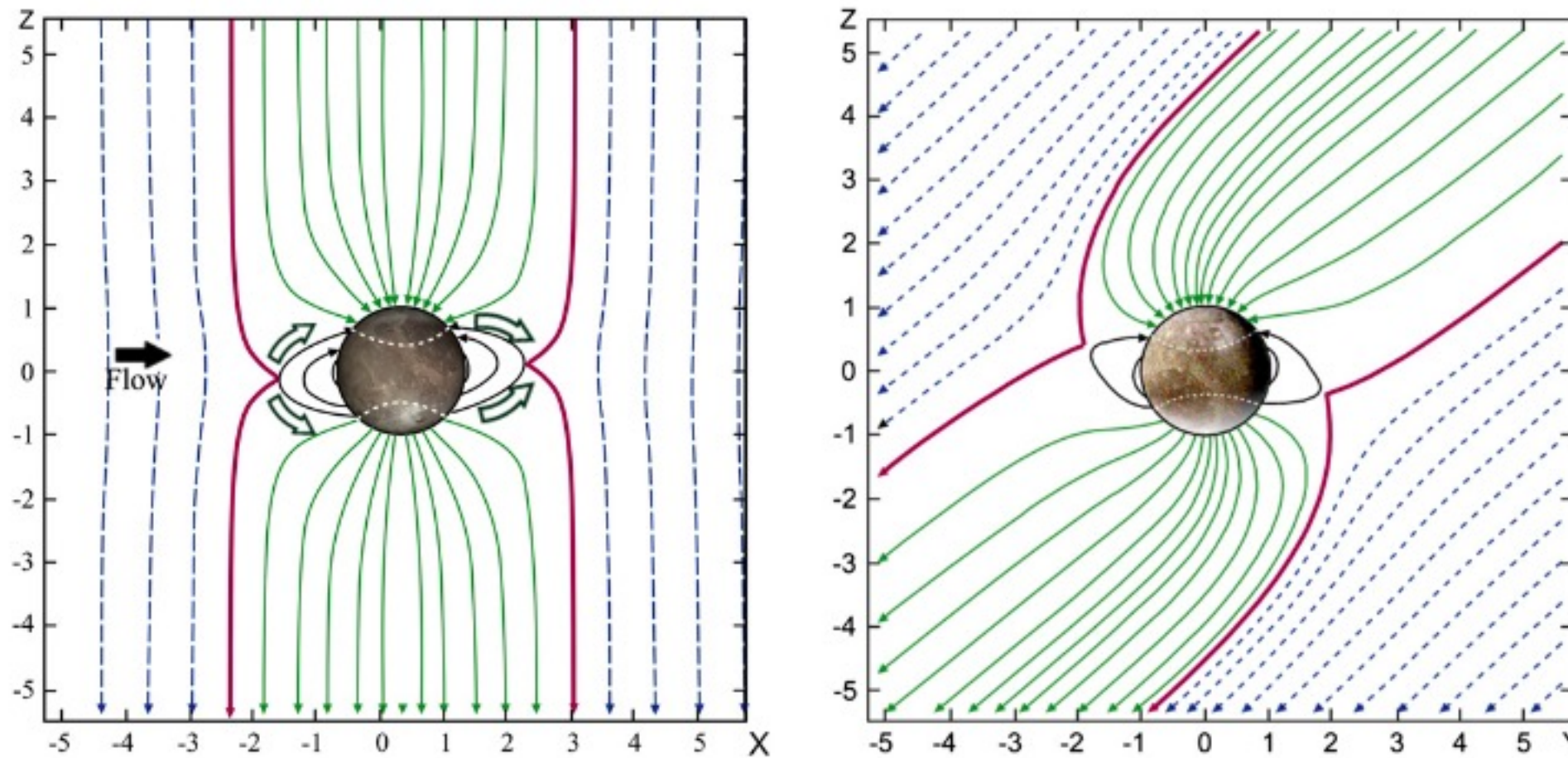


Fig. 1. The configuration of Ganymede's magnetosphere in the X–Z (left) and Y–Z (right) planes. The x-axis is parallel to the corotation direction (effectively parallel to the Ganymede orbital direction), y is positive inward toward Jupiter, and z is parallel to the spin axis of Jupiter (effectively parallel to the Ganymede spin axis). Red lines show the last fully open field lines that are connected at both ends to Jupiter. Open arrows mark the path of newly opened field lines, and the dark arrow marks the direction of jovian magnetospheric flow.

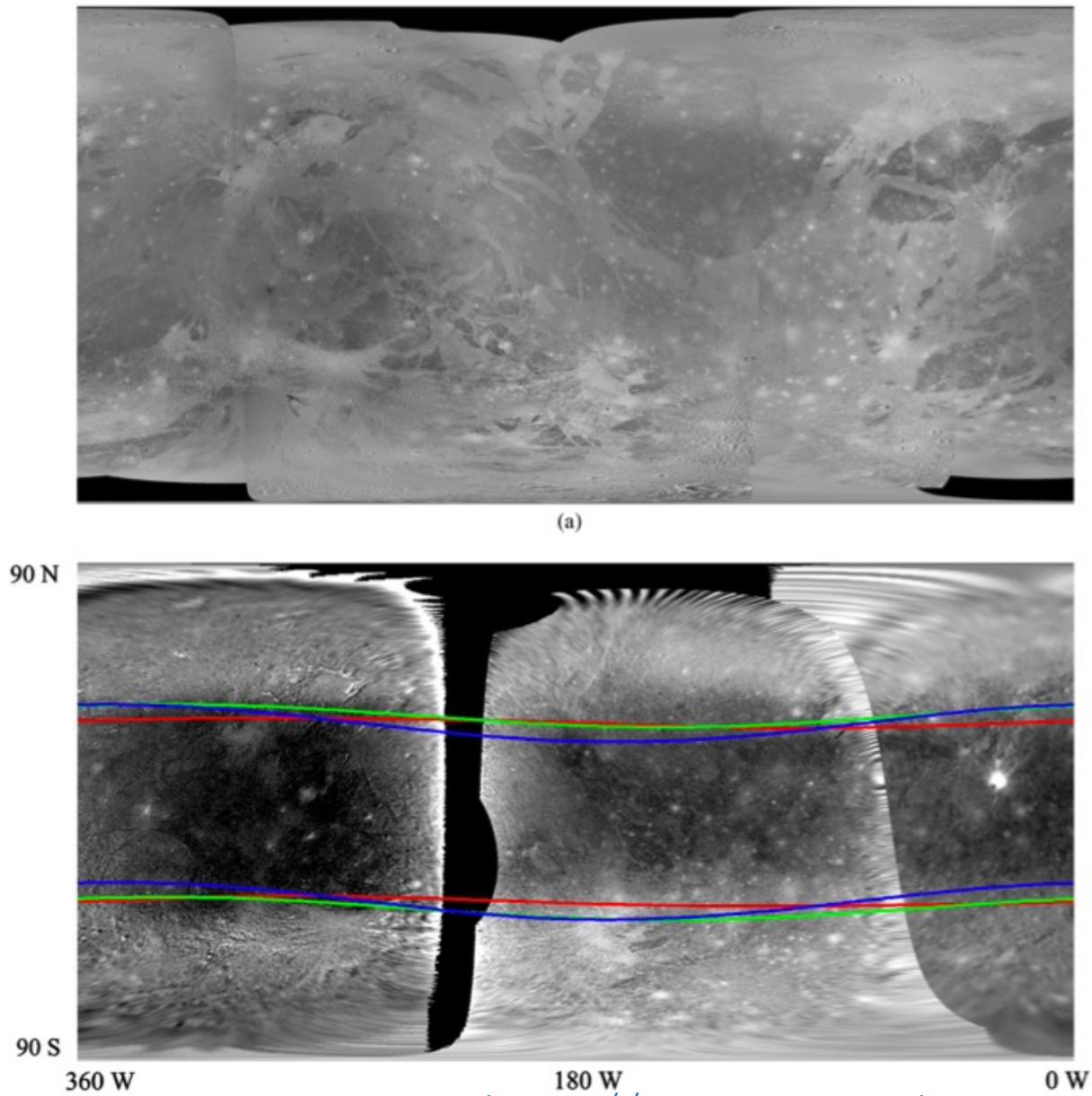


Fig. 3. Global image mosaics of Ganymede and predicted locations of the open/closed field line (OCFL) boundary. (a) Mosaic of Voyager and Galileo clear filter (broadband) images at a variety of resolutions. (b) Green/violet ratio composite image of Galileo color data from orbits E14 (west, 10.4 km/pixel), G1 (central, 13.1 km/pixel), and C10 (east, 7.3 km/pixel green and 14.7 km/pixel violet). Superimposed are the OCFL boundaries for three different configurations: red, when Ganymede is farthest above Jupiter's plasma sheet, green when Ganymede is located in the middle of the plasma sheet, and blue when Ganymede is located farthest below the plasma sheet. Image mosaics are in simple cylindrical projection and were produced by the U.S. Geological Survey, Flagstaff, Arizona.

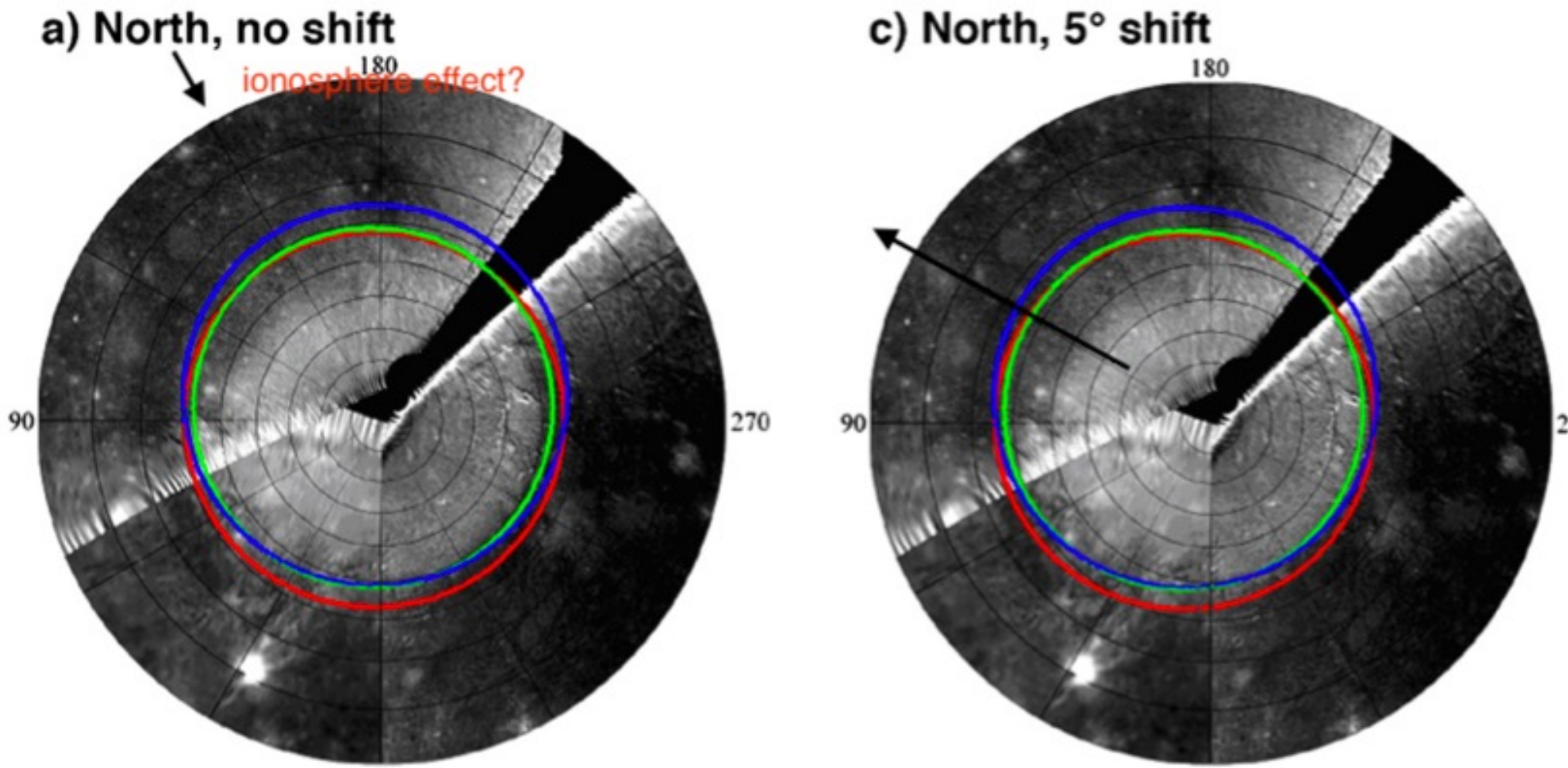


Fig. 4. Northern (a) and southern (b) polar projections of the Ganymede green/violet ratio image shown in Fig. 3b, and the corresponding OCFL boundaries obtained from field line mapping. The corresponding figures (c) and (d) are the same images but with the OCFL boundaries shifted by 5° in the direction of plasma flow; i.e., toward the leading point of the satellite's orbital motion (toward 90°W longitude).

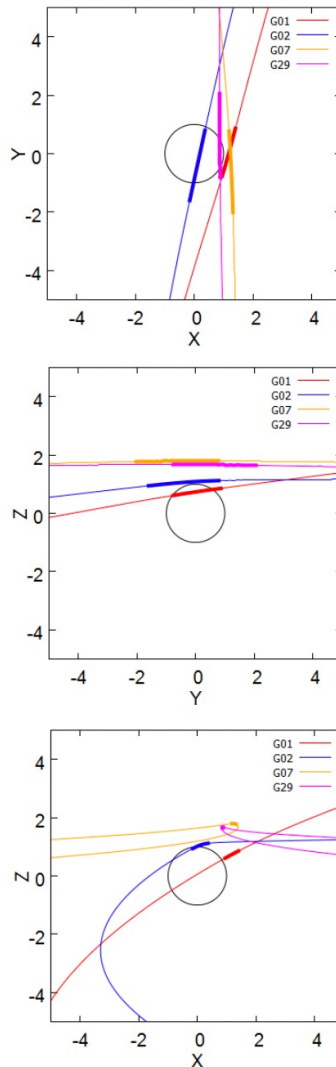


図 2.4 ガニメデ接近時のガリレオの軌道（細線）と、UHR 周波数の読み取りを行った時間に対応する軌道（太線）。上から XY 平面、YZ 平面、XZ 平面を示す。

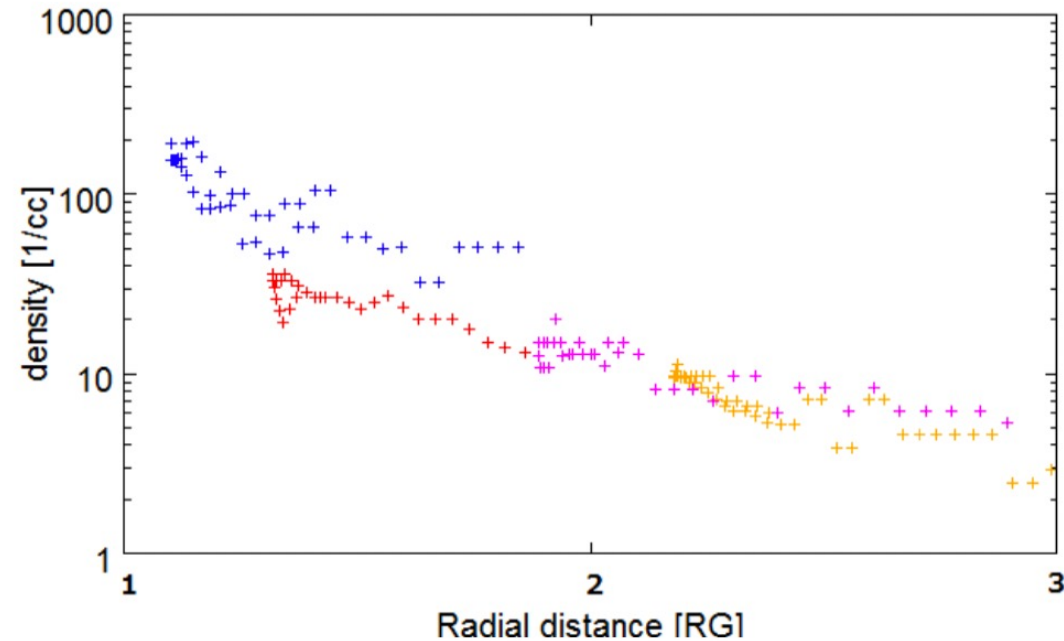
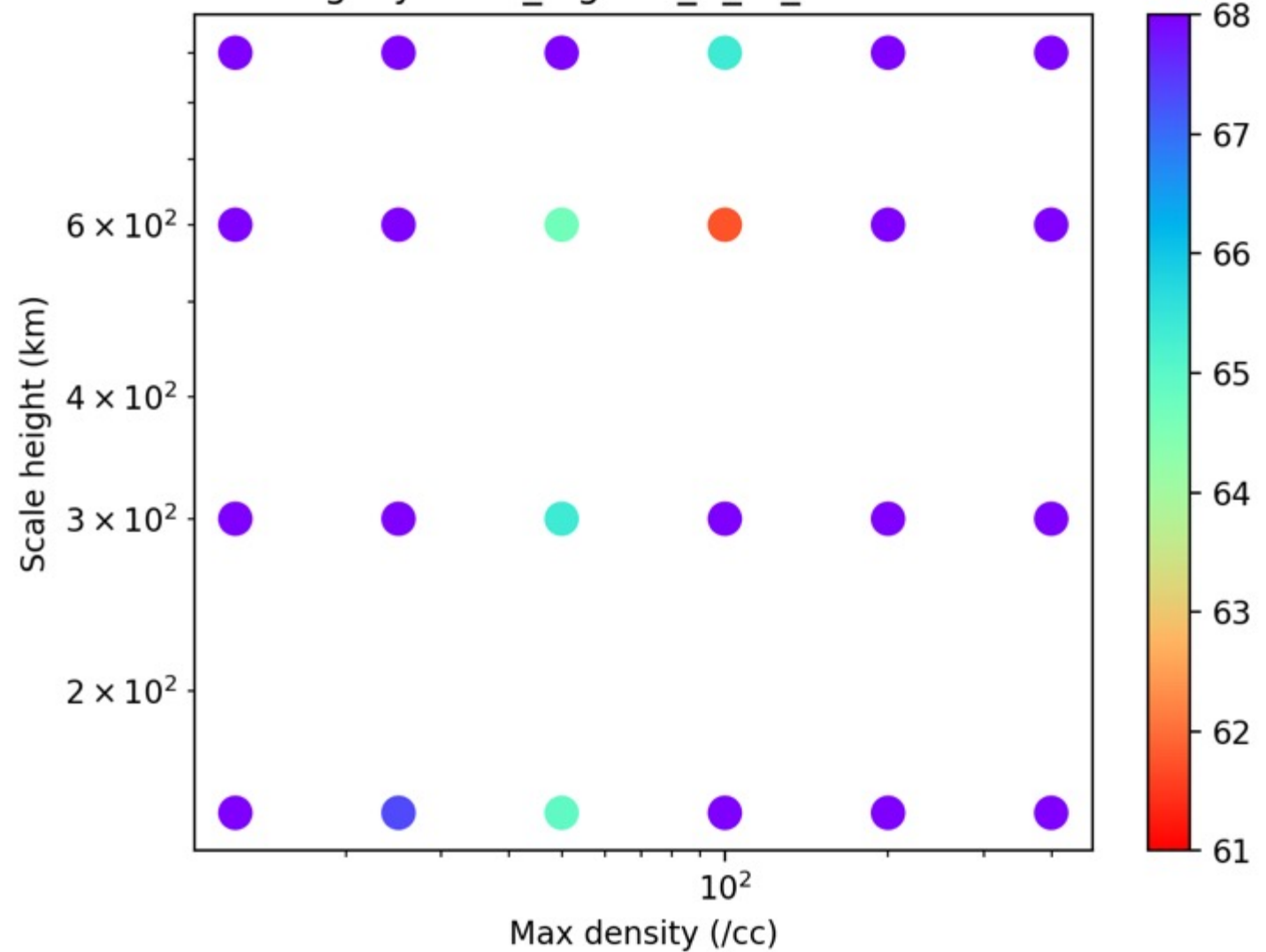
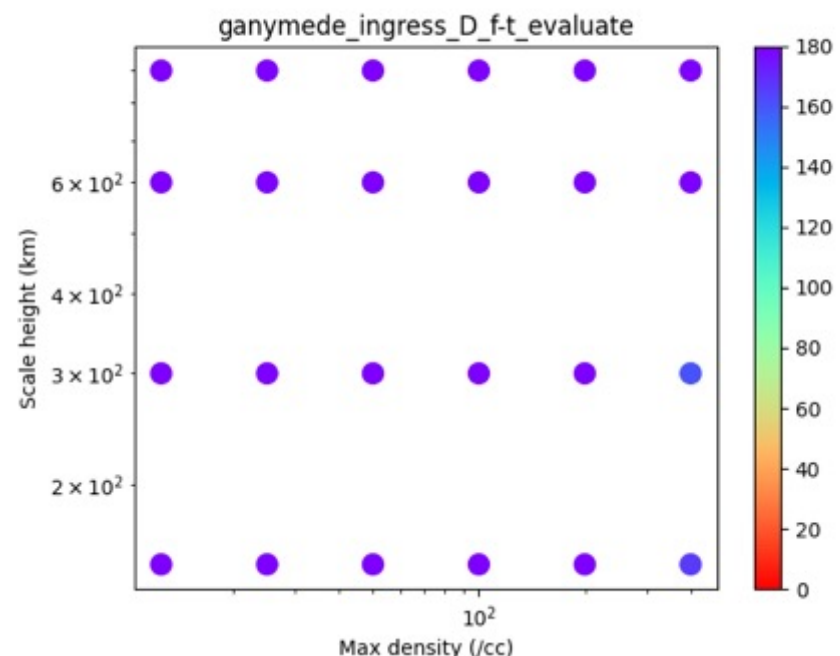
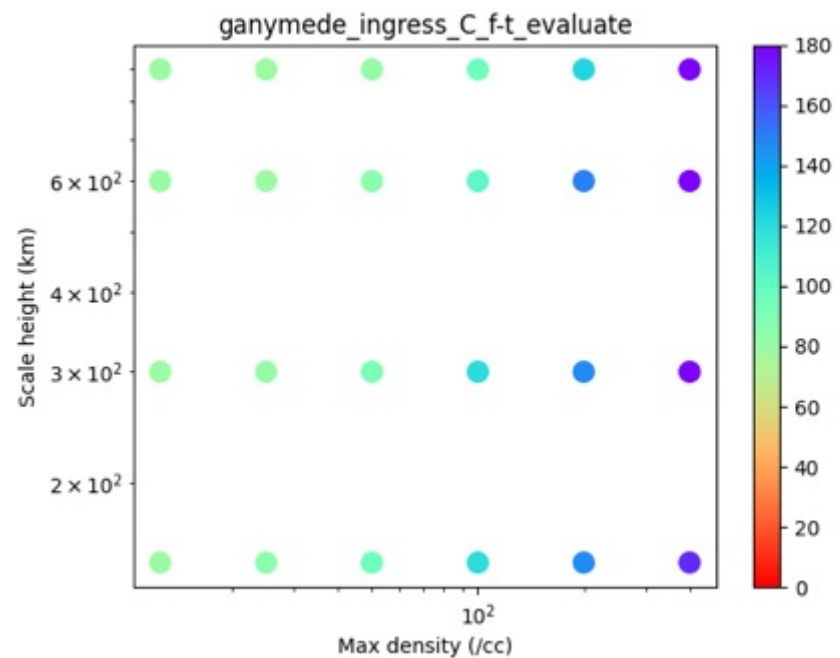
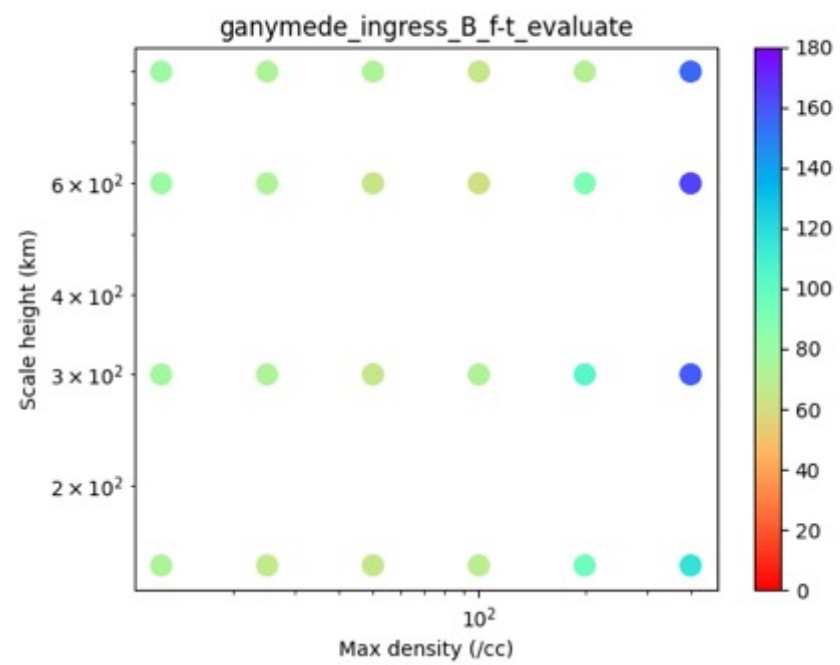
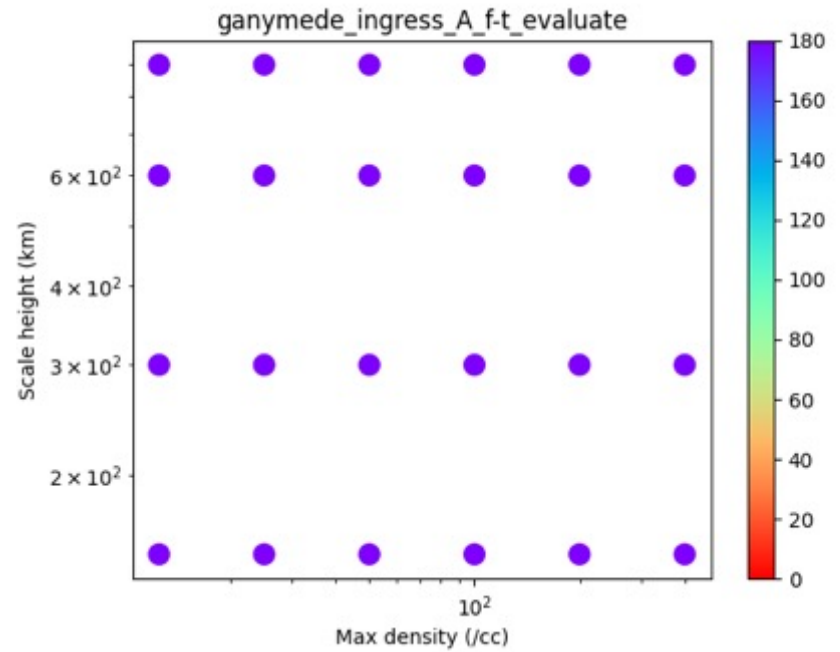


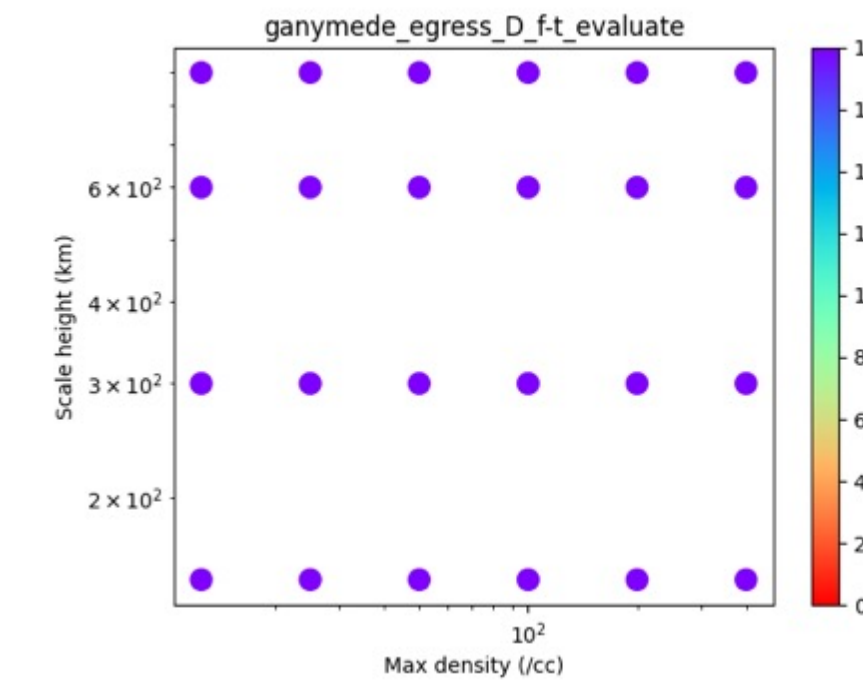
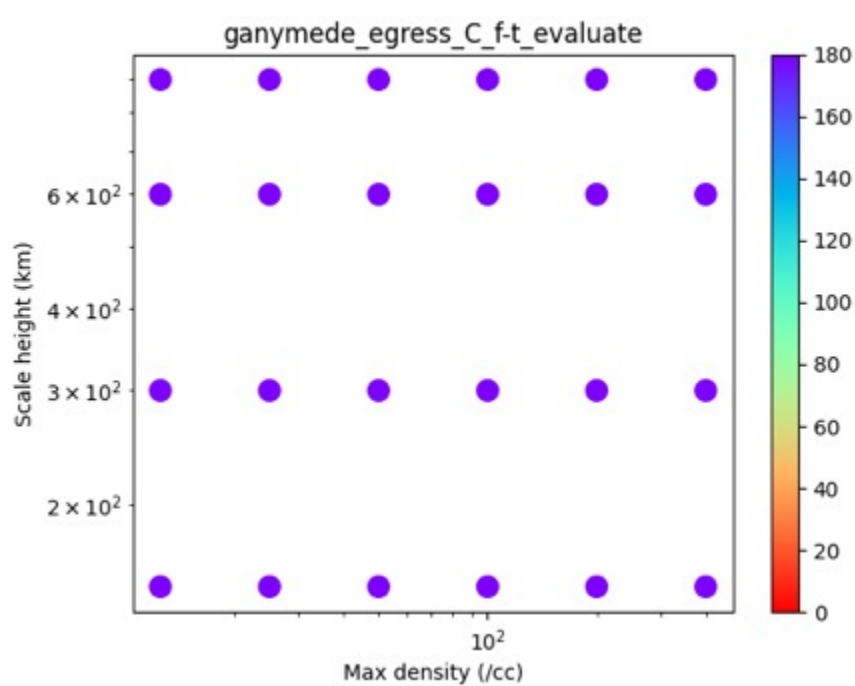
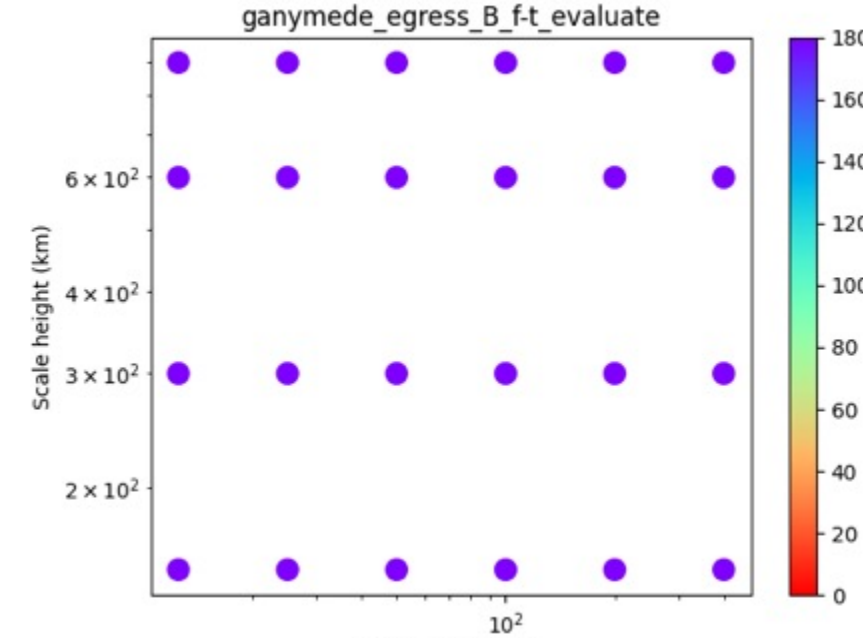
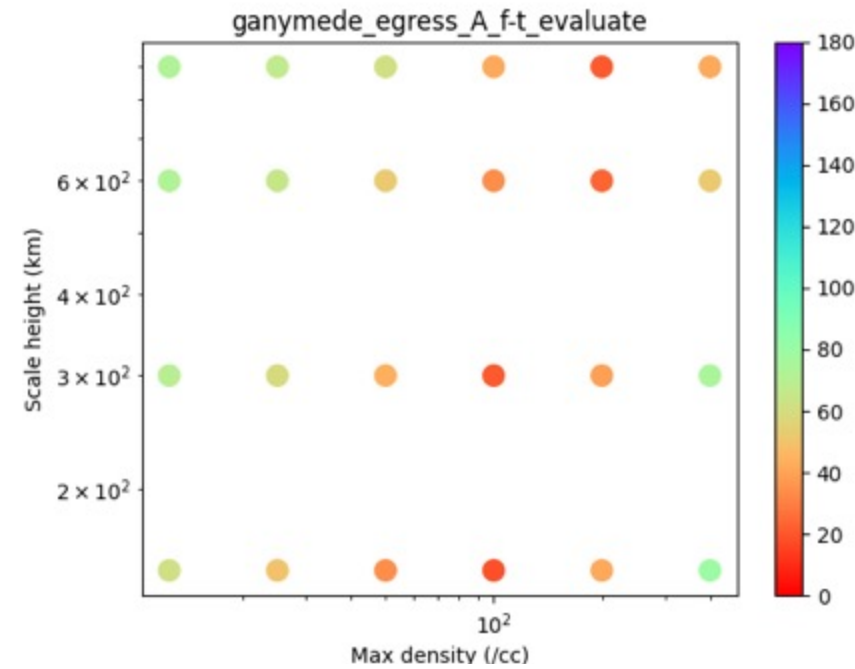
図 2.6 電子密度の動径方向距離変化。縦軸の電子密度は対数で表す。色は各軌道の違いを表す（赤…G01、青…G02、黄…G07、ピンク…G29）。

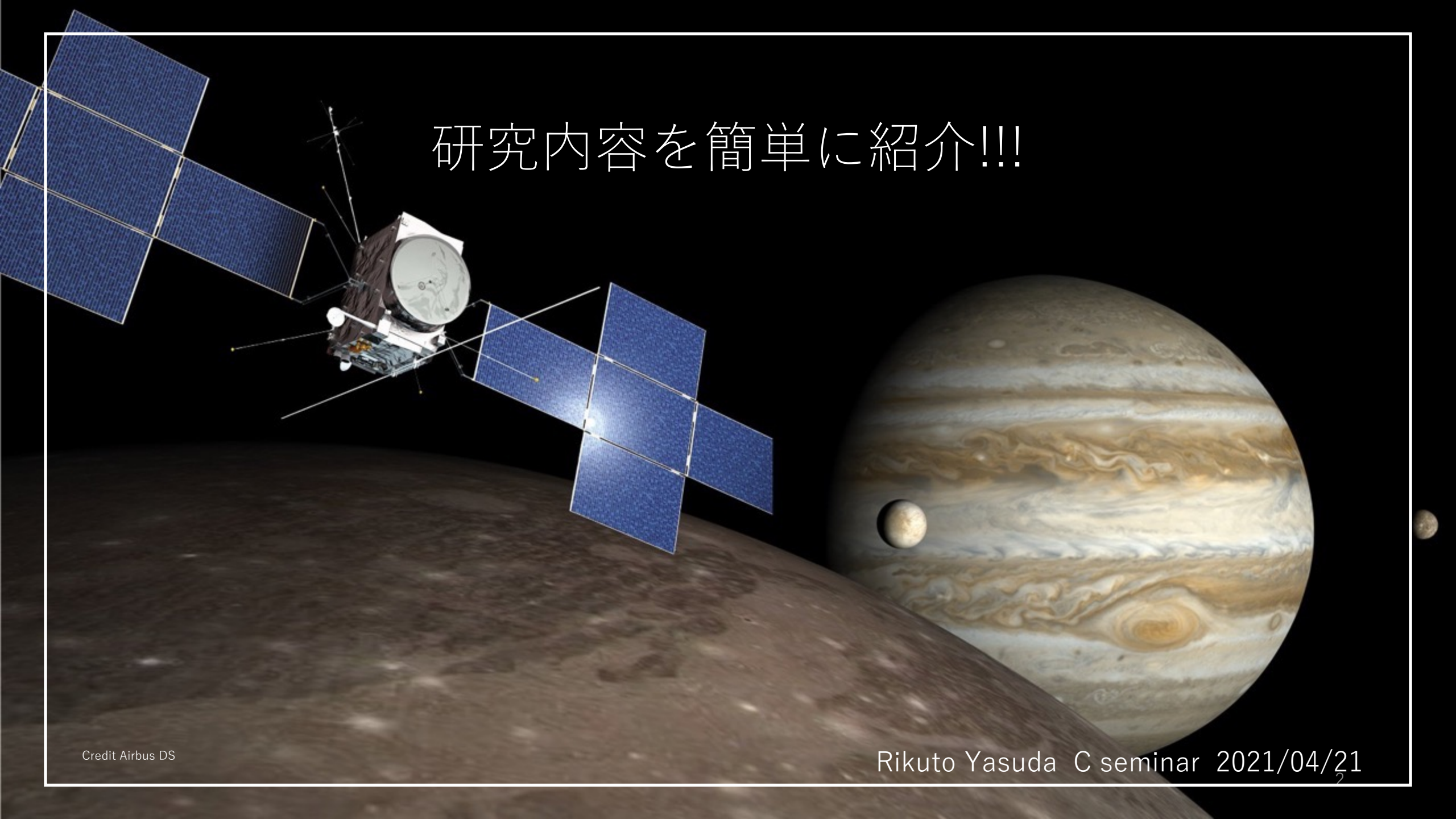
Orbit	T [K]	T [eV]
G01	1250	1.07×10^{-1}
G02	798	6.89×10^{-2}
G07	391	3.37×10^{-2}
G29	742	6.40×10^{-2}

ganymede_ingress_B_f-t_evaluate









研究内容を簡単に紹介!!!

研究対象 … 木星氷衛星

(エウロパ, ガニメデ, カリスト)

- 内部海の存在が示唆
 - 地球よりも多くの液体水を有する可能性
 - 生命が存在する可能性

調べたいもの … 大気構造・内部構造

- 大気構造
生命活動に欠かせないエネルギー (ex. 酸素)
の分布？
 - 内部構造
生命が存在しうる場所の特定

～研究テーマ～

木星から放射される電波を利用した 氷衛星内部・大気構造の観測手法の開発

なぜ、木星からの電波で氷衛星の大気構造・内部構造を調べられるの？



Fig.1 エウロパと地球の比較 (NASA)

觀測

理論

装置開発

火星

木星(衛星)

地球

太陽



Fig.2 漫画「ゆゆ式」三上小又作3巻 p 49より
(エウロバの話をしている回があったので貼ってみた。
この漫画読んだことある人に会ったことない..)



なぜ、木星からの電波で
氷衛星の大気構造・内部構造を
調べられる（かもな）の？

木星電波の通り道が氷衛星の大気や内部
の構造によって変わるから！（ \Leftrightarrow ）

Fig.3 アニメ「ふらいんぐういっち」のチトさん
(魔女の使い魔・ネズミは卒業したらしい・氷衛星とは全く関係ない)

1. 木星からの電波をシミュレーションで再現
2. 再現された電波の観測結果を予測
3. 観測結果と予測を比較して大気や内部の構造を推定

木星電波を利用した新たな
氷衛星内部・大気構造の観測手法を開発！



Fig.4 氷衛星の中性大気のイオン化プロセス
(adapted from NASA/JPL, Airbus DS and gcoe-earths.org)

